Universidad Nacional Autónoma de México

Facultad de Ciencias

Conjecture about the Quantum Chromodynamics phase diagram with two light quark flavors

T E S I S

que para obtener el título de:

físico

P R E S E N T A :

José Antonio García Hernández

tutor

Dr. Wolfgang Peter Bietenholz

Ciudad Universitaria, Cd. Mx., 2020

1. Datos del alumno
García
Hernández
José Antonio
Universidad Nacional Autónoma de México
Facultad de Ciencias
Física
414003789

2. Datos del tutor
Dr.
Wolfgang Peter
Bietenholz

3. Datos del sinodal 1
Dr.
Mariano
Chernicoff
Minsberg

4. Datos del sinodal 2
Dr.
Roelof
Bijker

5. Datos del sinodal 3
Dr.
Gabriela
Murguía
Romero

6. Datos del sinodal 4
Dr.
Eleazar
Cuautle
Flores

7. Datos del trabajo escrito
Conjecture about the Quantum Chromodynamics phase
diagram with two light quark flavors
80 p
2020

Resumen

La exploración del diagrama de fase de la QCD proporcionará una visión de varios sistemas. Por ejemplo, en el universo temprano se llevaron a cabo varias transisiones de fase donde una de ellas fue la transición del plasma de cuarks y gluones a la fase hadrónica. El plasma de cuarks y gluones puede también ser encontrado en colisiones de iones pesados realizados actualmente en el CERN y el RHIC.

En el límite quiral de la QCD con dos sabores de cuarks, su Lagrangiano tiene la misma simetría global O(4) que el iman de Heisenberg de cuatro componentes. Con cuarks masivos, la simetría O(4) es rota explícitamente. En el iman de Heisenberg, el mismo rompimiento explícito de simetría se introduce con un campo magnético externo. De esta manera, las simulaciones numéricas del modelo σ no lineal 3 dimensional con un campo magnético externo, proveerá un panorama del diagrama de fase de la QCD.

En este trabajo se explora el diagrama de fase de la QCD con el modelo sigma no lineal en tres dimensiones con un campo magnético externo y usando la carga topológica Q como el número barionico. Este modelo es usado como un modelo efctivo que evita el problema del signo que ha prevenido simulaciones numéricas a una alta densidad barionica.

Abstract

The exploration of the QCD phase diagram will provide insight of various systems. For instance, the early universe underwent several phase transitions, one of them being the transition from the quark-gluon plasma to the hadronic phase. The quark gluon plasma can also be found in heavy ion collision in experiments currently performed at CERN and RHIC.

In the chiral limit of QCD with 2 quark flavors, its Lagrangian has the same global O(4) symmetry as a four component Heisenberg ferromagnet. With massive quarks, the O(4) symmetry is explicitly broken. In the Heisenberg ferromagnet the same explicit symmetry breaking enters as an external magnetic field. Thus, the numerical simulation of the 3-d non-linear σ-model with an external magentic field will provide insight into the QCD phase diagram.

In this thesis we explore the 2-flavor phase diagram of QCD with the 3-d $O(4)$ model with an external magnetic field and using the topological charge Q as the *baryon number*. This model is used as an effective model which avoids the *sign problem* which has prevented numerical simulations at high baryon density.

Contents

Chapter 1

Theoretical Background

1.1 Path integral in Euclidean time

Feynman's path integral or functional integral [1, 2] formalism provides an alternative formulation to the canonical approach of quantum mechanics and reveals a connection between statistical mechanics and quantum theory.

We begin by defining the central quantity in statistical mechanics, the partition function (using units where $k_B = 1$)

$$Z = \mathrm{Tr} \exp(-\beta \hat{H}) = \int dx \, \langle x| \exp(-\beta \hat{H}) |x\rangle, \tag{1.1}$$

where $\beta = 1/T$ is the inverse temperature, $\hat{H}$ is the Hamilton operator and $|x\rangle$ is a position eigenstate. We will show that (1.1) is equivalent to a path integral in purely imaginary time.

First, take the definition of the propagator of a particle that comes back to its initial eigenstate $|x\rangle$,

$$\langle x|\hat{U}(t', t)|x\rangle = \langle x| \exp\left(-\frac{i}{\hbar}\hat{H}\,(t' - t)\right)|x\rangle. \tag{1.2}$$

This resembles the integrand of the definition of equation (1.1), and now we can relate the evolution operator $\hat{U}(t', t) = \exp\left(-\frac{i}{\hbar}\hat{H}(t' - t)\right)$ with the weight function

$\exp(-\beta\hat{H})$ in the partition function by

$$\beta = \frac{i}{\hbar}(t' - t) = \frac{1}{\hbar}(t'_{\mathrm{E}} - t_{\mathrm{E}}). \tag{1.3}$$

In the last expression we apply the transformation

$$t_E = it, \tag{1.4}$$

where t_{E} is known as the Euclidean time, which is obtained by a rotation of $\pi/2$ of the real time t in the complex plane. This is known as the *Wick rotation*, which has the benefit of getting rid of the factor i in the exponent of the path integral. In this sense, a system at finite temperature corresponds to a periodic propagation in Euclidean time.

If we divide the Euclidean time into N equidistant steps of length Δt_{E} by letting $\beta = N\Delta t_{\mathrm{E}}/\hbar$, and inserting a complete set of position eigenstates at all intermediate times $t_{\mathrm{E}_l} = t_{\mathrm{E}} + l\Delta t_{\mathrm{E}}$, $l = 1, 2, ..., N-1$, we arrive at

$$\begin{aligned}\langle x|\hat{U}(t'_{\mathrm{E}}, t_{\mathrm{E}})|x\rangle = \int dx_1 \int dx_2 \cdots \int dx_{N-1}\ \langle x|\hat{U}(t'_{\mathrm{E}}, t_{\mathrm{E}_{N-1}})|x_{N-1}\rangle \cdots \\ \cdots \langle x_2|\hat{U}(t_{\mathrm{E}_2}, t_{\mathrm{E}_1})|x_1\rangle\langle x_1|\hat{U}(t_{\mathrm{E}_1}, t_{\mathrm{E}})|x\rangle.\end{aligned} \tag{1.5}$$

Figure 1.1 illustrates this process, known as summing over paths.

Now we focus on one of these intermediate propagators. We consider a single particle of mass M moving in a potential $V(x)$. Its Hamilton operator reads

$$\hat{H} = \frac{\hat{p}^2}{2M} + \hat{V}(\hat{x}). \tag{1.6}$$

After some algebra, inserting a complete set of momentum eigenstates and cpomputing the integral over momenta, arrive at an expression for the intermediate propagator [2]

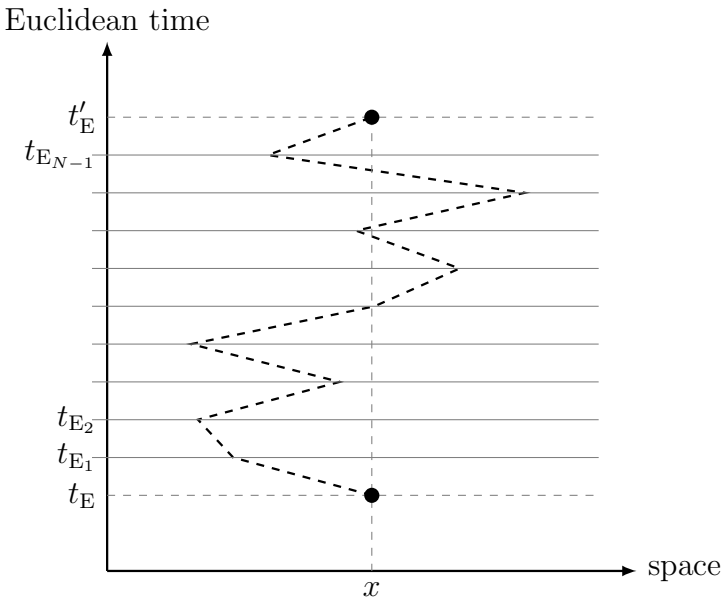

Figure 1.1: Illustration of the transition of a particle from (x, t_{E}) to (x, t'_{E}). Note the periodic boundary condition $|x\rangle = |x'\rangle$. The Euclidean time path integral is obtained by integrating over all possible positions at times $t_{\mathrm{E}_1}, t_{\mathrm{E}_2}, ..., t_{\mathrm{E}_{N-1}}$.

$$\langle x_{i+1}|\hat{U}(t_{\mathrm{E}i+1}, t_{\mathrm{E}i})|x_i\rangle = \left(\frac{M}{2\pi\hbar\Delta t_{\mathrm{E}}}\right)^{1/2} \exp\left(-\frac{1}{\hbar}\Delta t_{\mathrm{E}}\left[\frac{M}{2}\left(\frac{x_{i+1}-x_i}{\Delta t_{\mathrm{E}}}\right)^2 + \frac{1}{2}\left(V(x_i)+V(x_{i+1})\right)\right]\right). \tag{1.7}$$

Inserting this into equation (1.5) and inserting it again into the definition of the partition function (1.1) and taking the limit $\Delta t_{\mathrm{E}} \to 0$ we arrive at the *Euclidean time path integral*

$$\boxed{Z := \int dx\, \langle x|\hat{U}(t', t)|x\rangle = \int \mathcal{D}x \exp\left(-\frac{1}{\hbar}S_{\mathrm{E}}[x]\right).} \tag{1.8}$$

Now the action takes the Euclidean form

$$S_{\mathrm{E}}[x] = \int_0^\beta dt_{\mathrm{E}}\left[\frac{M}{2}(\partial_{t_{\mathrm{E}}}x)^2 + V(x)\right], \tag{1.9}$$

and the measure reads

$$\int \mathcal{D}x = \lim_{\Delta t_E \to 0}\left(\frac{M}{2\pi\hbar\Delta t_{\mathrm{E}}}\right)^{N/2} \int dx_1 \int dx_2 \cdots \int dx_N. \tag{1.10}$$

As in the case of the real time path integral, the dominant contributions to the integral are configurations where S_{E} is minimal, but here configurations of larger S_{E} are exponentially suppressed.

One advantage of the Euclidean path integral is that we can evaluate thermal expectation values. If we take an operator $\hat{O}(\hat{x})$ that is diagonal in the position basis $\{|x\rangle\}$, then the thermal expectation value of $\hat{O}$ is

$$\langle \hat{O}(\hat{x}) \rangle = \frac{1}{Z} \mathrm{Tr} \left[\hat{O}(\hat{x}) \exp(-\beta \hat{H}) \right] = \frac{1}{Z} \int \mathcal{D}x \; O(x(0)) \exp\left(-\frac{1}{\hbar} S_E[x] \right). \quad (1.11)$$

In this sense, if we have a quantum system, we can often turn it into a statistical mechanical problem by using the Euclidean time path integral and evaluate observables by computing their thermal expectation values. In order to compute a thermal expectation value as in eq. (1.11), we need to generate a set of configurations C weighted with probability distribution $p[C] = \frac{1}{Z} \exp(-\frac{1}{\hbar} S_{\mathrm{E}}[C])$. Therefore the expectation values will be of the form

$$\langle O \rangle \approx \frac{1}{\#\text{ of configurations}} \sum_{\text{configurations}} O[C]. \quad (1.12)$$

In Chapter 2, we will discuss in detail how to obtain such configurations.

1.2 Non-linear σ-models

Quantum Field Theory (QFT) is the generalization of point particle quantum mechanical systems to infinite degrees of freedom, combined with special relativity. A classical field $\Phi(x^\mu)$ is a function of space-time and can be quantized by means of the canonical quantization. On the other hand the path integral formalism makes use of the classical field.

Systems such as ferromagnetic materials, superfluids, thin films etc. can be described by *classical spin models*. Here the term spin does no refer to quantization of angular momenta, instead classical spins are used as statistical variables defined in a $\mathbb{R}^N$ — can also be $\mathbb{C}^N$— dimensional space. We work with these classical spins first by introducing a spatial d-dimensional lattice (in this thesis we will be working

with a 3-dimensional cubic structure with length L and volume $V = L^3$). Its sites will be labeled by the index x. The spins $\vec{e}_x$ are described by vectors defined in an intrinsic N-dimensional space $\vec{e}_x \in \mathbb{R}^N$, and are attached to the sites x of the spatial d-dimensional grid. Finally, we impose the non-linear constraint $|\vec{e}_x| = 1$. We usually denote this condition as $\vec{e}_x \in S^{N-1}$, meaning that the spins $\vec{e}_x$ are defined in the hypersphere S^{N-1}.

Systems which are described with these classical spins with the constriction $|\vec{e}_x| = 1$ that have a global O(N) symmetry are known as *non-linear σ-models* or *O(N) models*.

We can obtain the Lagrangian of a non-linear σ-model from the Lagrangian of the *linear σ-model* [3, 4] which is of the form

$$\begin{aligned}\mathcal{L}(\vec{\Phi}, \partial_\mu \vec{\Phi}) &= \frac{1}{2}\partial_\mu \vec{\Phi}^T \partial_\mu \vec{\Phi} + \frac{m^2}{2}\vec{\Phi}^2 + \frac{\lambda}{4}(\vec{\Phi}^2)^2 \\ &= \frac{1}{2}\partial_\mu \vec{\Phi}^T \partial_\mu \vec{\Phi} + \frac{\lambda}{4}\left(\vec{\Phi}^2 + \frac{m^2}{\lambda}\right)^2 + \text{const.}\end{aligned} \tag{1.13}$$

If we take $m^2 = -\lambda$ and let $\lambda \to +\infty$, we arrive at the Lagrangian of a non-linear σ-model,

$$\mathcal{L}(\vec{e}, \partial_\mu \vec{e}) = \frac{1}{2}\partial_\mu \vec{e}^T \partial_\mu \vec{e}. \tag{1.14}$$

We list some spin models depending on the spin dimension:

$N = 1$	Ising model	It can be used to describe ferromagnetism, a lattice gas or a first approximation to a neural network. Spins can take two discrete values, either 1 or -1. In $d > 1$ and infinite volume the model exhibits a second order phase transition.
$N = 2$	XY-model	Describes aspects of superfluids, thin films, etc. The spins live in the unit circle.
$N = 3$	Heisenberg model	This is the natural way of describing ferromagnetism.

$N = 4$	This work	In chiral perturbation theory with two quark flavors (up and down), the low energy dynamics of pions, can be described with a 3-d O(4) model. Due to the spontaneous symmetry breaking exhibited by the system, three quasi Nambu-Goldstone bosons (to be described in Section 1.5) represent the lightest particles involved, which in this case are indeed the pions.
$N = \infty$	Spherical model	This limit simplifies analytical calculations.

This kind of models are characterized by a *Hamilton function* $\mathcal{H}$, which specifies the energy of any spin configuration. Couplings between spins are often restricted to their nearest neighbors sites, which are denoted as $\langle xy \rangle$, including periodic boundary conditions. The standard form of the Hamilton function reads

$$\mathcal{H}[\vec{e}] = -J \sum_{\langle xy \rangle} \vec{e}_x \cdot \vec{e}_y. \tag{1.15}$$

$\mathcal{H}[\vec{e}]$ is a functional of the entire spin configuration, represented by the square brackets. J is the coupling constant, i.e. the strength of the interactions. We can add the term $-\vec{h} \cdot \sum_x \vec{e}_x$ to the Hamilton function which represents the presence of an external magnetic field $\vec{h} \in \mathbb{R}^N$. The presence of this term gives the spins in the lattice a preferred orientation in the direction $\vec{h}$. The external field breaks explicitly the intrinsic O(N) symmetry of the system. In fact, it breaks the symmetry down to O($N-1$).

The partition function of a classical spin model reads

$$Z = \int \mathcal{D}\vec{e} \, \exp\left(-\beta \mathcal{H}[\vec{e}]\right), \tag{1.16}$$

where the measure $\mathcal{D}\vec{e}$ means

$$\begin{aligned}\mathcal{D}\vec{e} &= \prod_x \int_0^\pi d\phi_1 \, \sin^{N-2}\phi_1 \cdots \int_0^\pi d\phi_{N-2} \, \sin\phi_{N-2} \int_0^{2\pi} d\phi_{N-1} \\ &= \prod_x \int_{-1}^1 de_x^1 \cdots \int_{-1}^1 de_x^N \, \delta(|\vec{e}_x| - 1)\,, \end{aligned} \tag{1.17}$$

where S^{N-1} is parametrized by the angles $\phi_1, \phi_2, \ldots, \phi_{N-1}$.

Thermal averages are computed as in equation 1.11. We list some important quantities in spin models

$$\text{energy density } \epsilon = \frac{1}{V}\langle\mathcal{H}\rangle \tag{1.18}$$

$$\text{specific heat } c_v = \frac{\beta^2}{V}\left(\langle\mathcal{H}^2\rangle - \langle\mathcal{H}\rangle^2\right) \tag{1.19}$$

$$\text{magnetization } M = |\langle\vec{M}\rangle|,\ \vec{M} = \sum_x \vec{e}_x \tag{1.20}$$

$$\text{magnetization density } m = \frac{1}{V}M \tag{1.21}$$

$$\text{magnetic susceptibility } \chi_m = \frac{\beta}{V}\left(\langle\vec{M}^2\rangle - \langle\vec{M}\rangle^2\right) \tag{1.22}$$

$$\text{spin-spin correlation function } \langle\vec{e}_x \cdot \vec{e}_y\rangle = \frac{1}{Z}\int \mathcal{D}\vec{e}\, \vec{e}_x \cdot \vec{e}_y \exp\left(-\beta\mathcal{H}[\vec{e}]\right) \tag{1.23}$$

$$\text{connected time layer corr. func. } C(r) = \langle\vec{s}_{x_3} \cdot \vec{s}_{x_3+r}\rangle - \langle\vec{s}_{x_3}\rangle \cdot \langle\vec{s}_{x_3+r}\rangle \tag{1.24}$$

$$\vec{s}_{x_3} = \frac{1}{L^2}\sum_{x_1,x_2} \vec{e}_{(x_1,x_2,x_3)}$$

$$C(r) \propto \exp\left(-\frac{r}{\xi}\right)$$

where ξ is the *correlation length*.

In Chapter 2 we will give different definitions for the magnetization density and the magnetic susceptibility. This is done in order to deal with a finite system using a computer.

In Section 1.1, we described a connection between statistical physics and quantum mechanics. With classical spin models we now establish a correspondence with some of the terminology of quantum field theory.

From now on we will work with units where $\hbar = 1$. In a quantum mechanical

system the path integral (sum over paths $[x]$) $\int \mathcal{D}x$ is defined in a 1-dimensional discrete Euclidean time, while in a spin model the sum over spin configurations $\int \mathcal{D}\vec{e}$ is defined in a spatial d-dimensional lattice. The Euclidean action $S_{\mathrm{E}}[x]$ corresponds to $\beta\mathcal{H}[\vec{e}]$. The function $\exp(-S_{\mathrm{E}}[x])$ weights paths while the Boltzmann factor $\exp(-\beta\mathcal{H}[\vec{e}])$ weights spin configurations. A 1-point function or *condensate* corresponds to the magnetization density $m = |\langle\vec{e}\rangle|$. The 2-point function corresponds to the spin-spin correlation function $\langle\vec{e}_x \cdot \vec{e}_y\rangle$. The inverse correlation length $1/\xi$ in a spin system is equal to the energy gap ΔE between the ground state and the first excited state in a quantum system. In particle physics this gap is the mass of the lightest particle involved.

1.3 Phase transitions and critical phenomena

When all the physical properties of a substance are uniform we say that the system is in a phase. For instance, water can be found in its liquid phase, the solid phase (ice) and a gaseous one (vapour). A substance can undergo a *phase transition*, which implies a drastic change of the properties of the system. This is achieved by changing some of its thermodynamic properties such as temperature, pressure, chemical potential etc. If we plot thermodynamic properties against one another, we have a graph called a *phase diagram*. A phase diagram specifies the state of the substance at each point. Two important features are considered, phase boundaries which are represented as coexistence curves of the phases, and *critical points* that is where a coexistence curve ends; also, there are lines and surfaces of critical points. Figure 1.2 shows a phase diagram of a pure substance (like water). We observe that the red lines separate distinct phases, in particular, one line ends in a *critical point*. For a detailed explanation on this subject we refer to Ref. [5].

An *order parameter* is a quantity that can distinguish between phases; it is zero when the system is in one phase (normally when the temperature is above the critical temperature T_c) and non-zero in the other. An example of an order parameter is the magnetization in a ferromagnetic substance. The magnetization indicates the difference between the magnetic (broken) phase $T < T_c$ and the non-

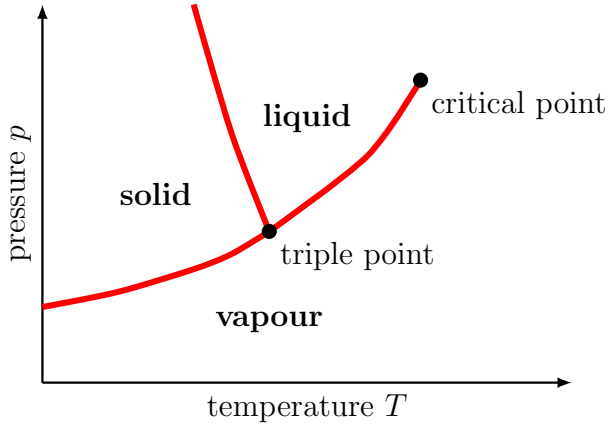

Figure 1.2: A typical p-T phase diagram of a pure substance. Red lines represent the coexistence curves. The black points represents a triple point, where three phases coexist, and the critical point, where a first order line ends.

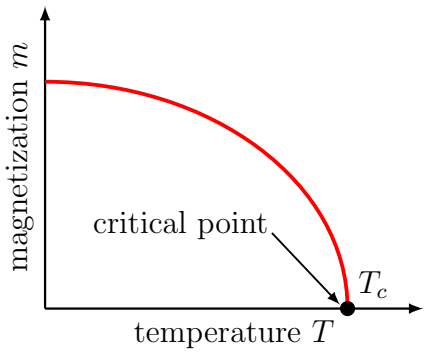

Figure 1.3: The magnetization m of a ferromagnetic material as the order parameter. The phase transition occurs at the critical temperature T_c.

magnetic (symmetric) phase $T \geq T_c$ (see figure 1.3).

Mathematically speaking, phase transitions are classified by an order n, which determines the lowest order of a derivative of a function where the function becomes discontinuous. If the n-derivative of a function — in thermal systems one usually deals with the free energy $F = -T \ln Z$ — with respect to the driving parameter — which in this case is the temperature T — is discontinuous we say that the phase transition is of order n. This way of defining phase transitions as discontinuities is known as the Ehrenfest scheme. The particular case where every n-order derivative is continuous is called an essential phase transition.

1.4 Critical exponents and universality

Critical exponents characterize the behaviour of physical quantities in the vicinity of a second order phase transition.

Let us refer to a ferromagnetic system. The magnetization M in the thermodynamic limit ($V \to \infty$) takes the form

$$M = -\left.\frac{\partial F}{\partial h}\right|_{T,h=0}. \tag{1.25}$$

As we mentioned earlier, M vanishes at and above the critical temperature T_c. First, we consider the magnetization M as T approaches T_c from below, at $h = |\vec{h}| = 0$. The behaviour is characterized by

$$\lim_{T \to T_c} M \propto (T_c - T)^{\beta}. \tag{1.26}$$

This relation is an ansatz, which introduces β as our first critical exponent (not to be confused with the inverse temperature). On the other hand, both the specific heat c_v and magnetic susceptibility χ_m diverge as $T \to T_c$. The definition and power laws for both read

$$\begin{aligned} c_v &= \left.\frac{T}{V}\frac{\partial S}{\partial h}\right|_{h=\text{const.}} &&= -\left.\frac{T}{V}\frac{\partial^2 F}{\partial T^2}\right|_{h=\text{const.}} &&\propto |T - T_c|^{-\alpha} \\ \chi_m &= \left.\frac{1}{V}\frac{\partial M}{\partial h}\right|_{h=0} &&= -\left.\frac{1}{V}\frac{\partial^2 F}{\partial h^2}\right|_{h=0} &&\propto |T - T_c|^{-\gamma} \end{aligned}$$

where $S = -\left.\frac{\partial F}{\partial T}\right|_{h=\text{const.}}$ is the entropy. The parameters α, β and γ are all critical exponents. If these exponents are the same among different systems, we say that they coincide within a universality class.

A *crossover* can be defined as a smooth transition between two phases. A crossover cannot be associated with a change of symmetry or a discontinuity in the free energy F, although there is a drastic change in phases. Typically it occurs in a region of the phase diagram rather than a single point. In a crossover the system changes from one type of critical behavior to another. We refer to [5] for this topic.

1.5 Spontaneous Symmetry Breaking

An order parameter is often related to the spontaneous or explicit break-down of a global symmetry, and can distinguish between the broken phase and the unbroken symmetry phase. When the Lagrangian of a system is symmetric with respect to a group of transformations, but the vicinities of a ground states do not exhibit the same symmetries, we say that the system undergoes a process known as *Spontaneous Symmetry Breaking* (SSB).

A process of SSB occurs in a ferromagnetic model; the system has a symmetry under some rotations, but the ground state is not invariant under the same rotations. If we deal with a classical spin model, then the Hamilton function (1.15) has a symmetry under transformations of the group O(N), i.e. transformations under spin rotations. For temperatures below the critical value, $T < T_c$, the "magnetized" or "ordered" configurations — where spins have a tendency to be aligned in some direction — dominate the path integral. In figure 1.4a we have a typical magnetized configuration, for instance, where spins point upwards. Here, the magnetization also points upwards, but after a rotation of π, the spins, and therefore also the magnetization, now point downwards. In this case, we say that the symmetry is broken. The alignment is destroyed by thermal fluctuations when $T \geq T_c$. Above the critical temperature, $T > T_c$, the non-magnetized or "disordered" configurations dominate the path integral where the spins point in random directions, there is no preferred orientation, see figure 1.4b. Here the magnetization vanishes and after the same rotation of π, the magnetization remains zero, such that the symmetry is restored.

SSB have numerous consequences; we list the most important in our project:

- **Phase transitions**[1]

  Different phases of a system are characterized by different kinds of symmetry, and are driven by different parameters (temperature, magnetic or electric field etc.). If the driving parameter is temperature, at high temperature, the

[1]Smooth phase transitons (of order ≥ 2) are often related to SSB, but not always. In the 2-d XY-model, by the Mermim-Wagner theorem [6, 7], SSB of the global $O(2)$ symmetry cannot occur. However, the system exhibits an essential phase transition known as the Berezinskii-Kosterlitz-Thouless transition.

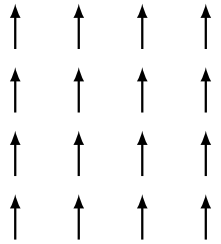

(a) Ground state, broken phase ($T < T_c$).

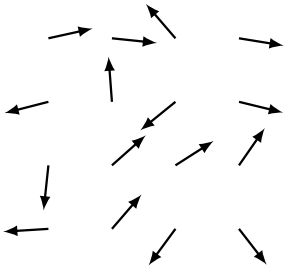

(b) Symmetric phase ($T > T_c$).

Figure 1.4: At low temperature ($T < T_c$) the spin system tends be in a phase of broken $O(N)$ symmetry (left), whereas at high temperature, strong thermal fluctuations remove preferred orientations so that the symmetry is restored (right).

system takes on a "higher degree of symmetry" phase; at lower temperatures, the phase is of a lower symmetry or "broken symmetry".

- **Nambu-Goldstone Bosons**

  When a system undergoes a spontaneous breakdown of a continuous global symmetry, some excitations of a vacuum (or ground state) of the system appear as massless particles known as *Nambu-Goldstone Bosons* (NGBs). One important feature of NGBs is that they can only appear in more than two space-time dimensions [6, 7].

1.6 The Standard Model

The building blocks of all visible matter in the universe are called elementary particles. The *Standard Model* (SM) is the theory that describes the interactions between elementary particles. However, only three of the four fundamental interactions, or forces, are described by the Standard Model, namely, electromagnetism, the weak force and the strong force [2].

The *fermions* is a set of particles which are characterized by a semi-integer spin, in the case of the elementary particles is 1/2. The elementary particles that conform fermionic matter are separated into two main subsets, the *leptons* and the *quarks*. Each set consists of six types of particles, that at the same time are structured into three *generations*.

[2]Unfortunately, since a quantum theory of gravitation is not well established, gravity and its hypotetical force carrier boson particle, the *graviton*, is not part of the Standard Model.

The first generation of quarks contains the flavors *up* (u) and *down* (d), and the first generation of leptons involves the *electron* (e) and the *electron neutrino* (ν_e). The first generation consists of the lightest particles. These are the ones — except ν_e — that gather together with electrons to form atoms, therefore all observable matter. The mass of an atom consists mostly of *nucleons* which contain three valence quarks, namely (udd) neutrons and (uud) protons.

The other large set corresponds to the *bosons* which are characterized by their integer spin. Interactions between elementary particles are mediated by the exchange of *gauge bosons*, which have spin 1, and by Yukawa couplings. The exchange of photons gives rise to the electromagnetic interaction, while the exchange of $W^{\pm}$ and Z bosons gives rise to the weak interaction. All elementary fermions of the SM can experience both of these iteractions — except for the neutrinos, which are electrically neutral —, since they carry electric charge weak hypercharge. However the strong interaction, which is mediated by gluons, is only experienced by quarks, since they are the only fermions with color charge. The last ingredient in the Standard Model is the *Higss field* which is the direct responsible for the mass of the gauge bosons Z and $W^{\pm}$, and through Yukawa couplings gives mass to all fermions. The remaining degree of freedom after the *Higgs mechanism* [8, 9] is known as the *Higgs boson*, which is a scalar boson with spin 0. Figure 1.5 shows the elementary particles in the Standard Model, along with their mass, electric charge and spin.

The mathematical description of the Standard Model relies on group theory. Each gauge interaction is represented by a local symmetry group, for instance, $U(1)$ represents the electromagnetic interaction, $SU(2)$ the weak interaction, and $SU(3)$ the strong interaction. Moreover, the generators of the groups represents the gauge bosons of each interaction. So, the whole gauge group of the Standard Model is $SU(3) \otimes SU(2) \otimes U(1)$.

1.7 The QCD Phase Diagram

It is known that hadronic matter undergoes a kind of phase transition from the hadronic phase to one where quarks and gluons are deconfined, known as the

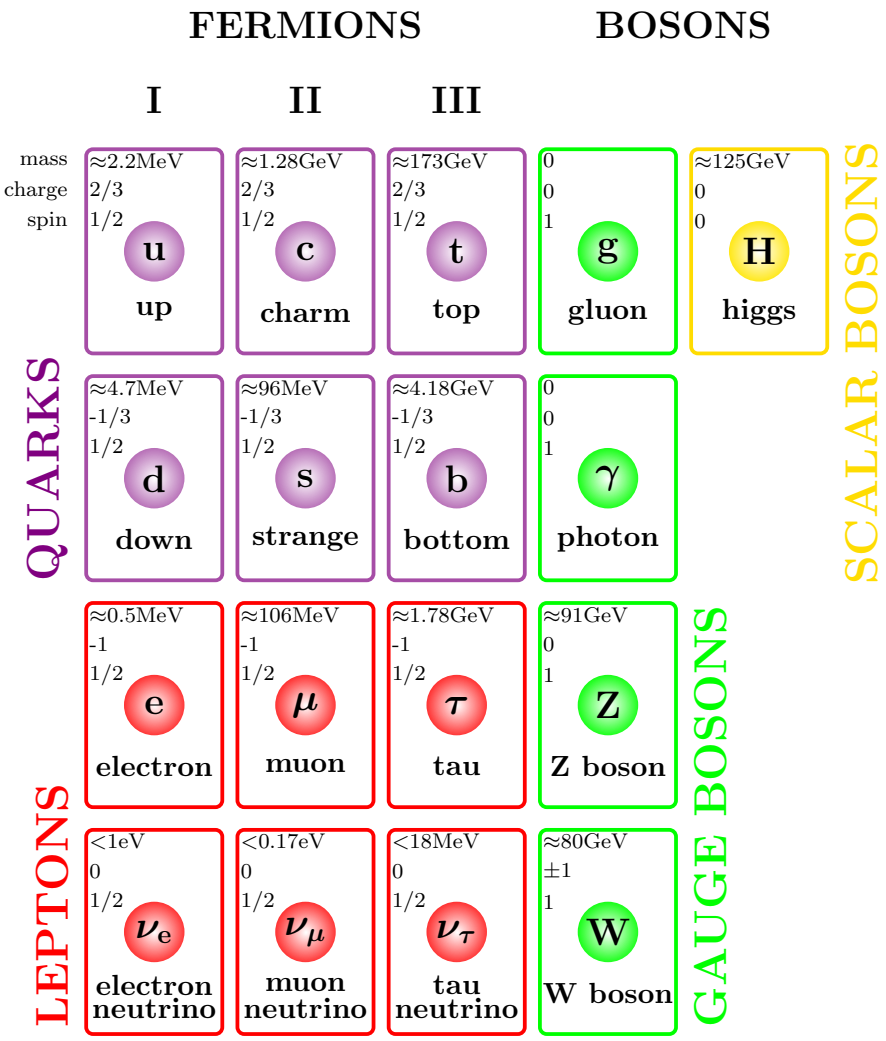

Figure 1.5: Standard Model of Elementary Particles.

quark-gluon plasma.

At low energies the SM can be described by Quantum Chromodynamics (QCD), the $SU(3)$ gauge theory of the SM. This is due to the fact that the inctrisct QCD scale $\Lambda_{\text{QCD}} \approx 200\text{MeV}$ is much more less than the vacuum expectation value of the Higss field $v_{\text{Higgs}} \approx 246\text{GeV}$.

QCD, which is the theory of strong interactions between quarks and gluons, with two massless quark flavors is often a reliable description of subnuclear physics at low energies. Its Lagrangian has a global chiral flavor symmetry $SU(2)_L \otimes SU(2)_R$ which can break spontaneously down to $SU(2)_{L=R}$. In this case we are in the confined phase, where quarks and gluons form hadronic matter. At high temperatures, chiral symmetry is restored and the system becomes a quark-gluon plasma. The order parameter of the breakdown is the chiral condensate.

If we consider the two lightest quark flavors (up and down) as massless, it is believed that the temperature (T) vs. chemical potential (μ_B) phase diagram ends at a particular critical point that separates a critical line of second order phase transitions from a line of first order phase transitions. This point is known as the *Critical End Point* (CEP). If we consider instead massive quarks, the critical line of second order phase transitions turns into a crossover line.

Little progress has been achieved in the task of exploring the phase diagram at high baryon density. Experiments at RIHC (Relativistic Heavy Ion Collider) and at CERN (Organisation Européenne pour la Recherche Nucléaire) have observed the quark-gluon plasma phase in heavy ion collisions, but the plasma occurs for a short time ($\sim 10^{-25}$ secs) before spontaneously condensing into hadrons [10].

A *super conductor color phase* [11] similar to the electrical superconductivity is also expected in the phase diagram. At high densities quarks could condense into Cooper pairs forming this new phase, but still breaking the chiral symmetry.

Lattice QCD is a powerful non-perturbative approach to solve QCD problems when perturbative calculations and other analytic approaches do not provide conclusive results. However the notorious sign problem has prevented numerical lattice QCD simulations at high baryon density. In Chapter 2 we will return to this subject.

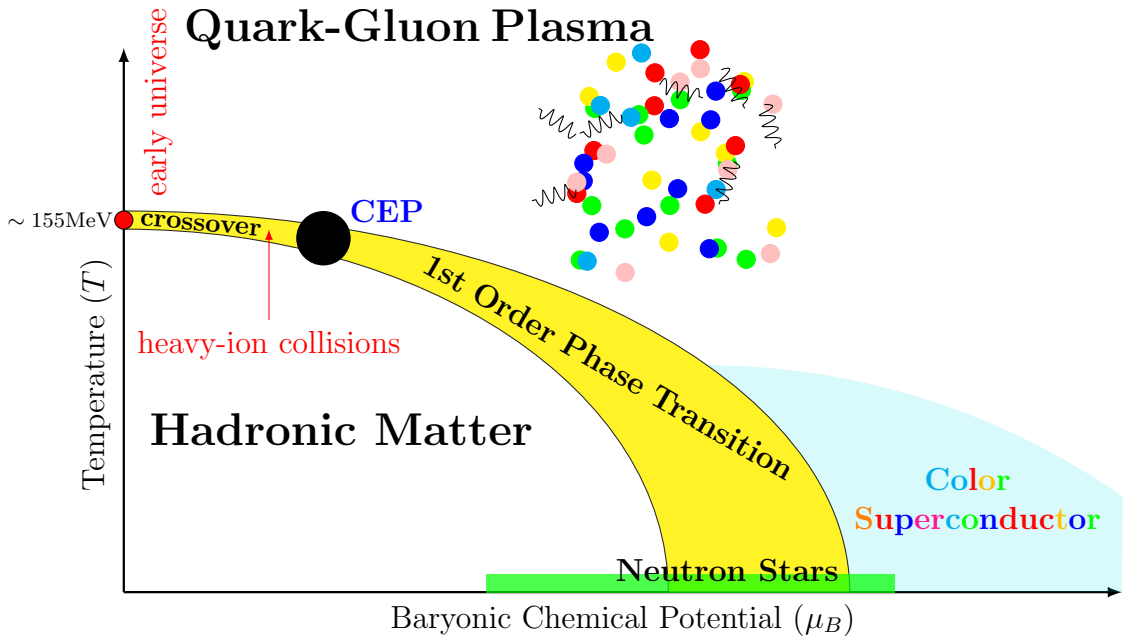

Figure 1.6: Conjectured QCD phase diagram.

The QCD phase diagram is not just of theoretical interest, since this phase transition may have occurred a few moments after the *big bang*, approximately $\sim 10^{-6}$ s [12], and neutron stars are believed to have a high baryon density, greater than $(0.5-1)$ nucleon/fm^3 [13]. Figure 1.6 shows a general overview of the conjectured QCD phase diagram with two massive quark flavors.

Chapter 2

Monte Carlo Methods

Monte Carlo methods are a broad class of statistical methods to approximate a quantity through random sampling processes. In particular, it is the only efficient way to compute high dimensional integrals. In this chapter we will focus on simulations of statistical mechanics problems.

In statistical mechanics we typically try to compute the thermal average of an ensemble, for instance, the canonical ensemble of a quantity O,

$$\langle O \rangle = \frac{1}{Z} \sum_C O[C] e^{-\beta H[C]} = \frac{\sum_C O[C] e^{-\beta H[C]}}{\sum_C e^{-\beta H[C]}}, \tag{2.1}$$

where

C: configuration of the system

$H[C]$: energy of the system in configuration C

$p[C] \equiv \frac{1}{Z} e^{-\beta H[C]}$: the probability of finding the system in one of the configurations C with energy $H[C]$.

In large systems the direct computation of $\langle O \rangle$ is not feasible, therefore we need to generate a representative set of configurations that have dominant contributions to the sum. The goal of our Monte Carlo method is to choose randomly a number N of configurations $\{C_1, C_2, \ldots, C_N\}$ which follow the probability density function

$$p[C] = \frac{1}{Z} e^{-\beta H[C]} \,. \tag{2.2}$$

We define the estimator O_N of $\langle O \rangle$ as

$$O_N = \frac{1}{N} \sum_{i=1}^{N} O[C_i] \,, \tag{2.3}$$

so that in the limit $N \to \infty$, we have $O_N \to \langle O \rangle$. We refer to Ref. [14] for this topic.

The question arises, how do we generate configurations C_i such that they follow the canonical ensemble? Commonly, *Markov chains* are used to generate them.

2.1 Markov chains

A stochastic process is a sequence of random events (configurations, states, etc.) in a chain-like manner that transits from one event to another. A *Markov chain* is a stochastic process where a subsequent event depends only in the current state of the system.

For the chain to be adopted to the canonical distribution as $N \to \infty$, it has to satisfy two conditions:

- **Ergodicity**: Every configuration can be reached in a finite number of steps. In other words, there exists a path from any C_i to any C_j.

- **Detailed balance**: This condition involves the probability transition $W[C \to C']$ of going from one configuration C to another C', the reverse $W[C' \to C]$, and the probabilities of these configurations $P[C]$ and $P[C']$. Detailed balance is a condition for the ratio between these quantities,

$$\frac{W[C \to C']}{W[C' \to C]} = \frac{P[C']}{P[C]}. \tag{2.4}$$

  For the canonical ensemble the probability of the configuration is given by eq. (2.2), so the detailed balance condition reads

$$\frac{W[C \to C']}{W[C' \to C]} = \frac{\frac{1}{Z} e^{-\beta H[C']}}{\frac{1}{Z} e^{-\beta H[C]}} = \exp\left(-\beta \Delta H\right),$$

  where $\Delta H = H[C'] - H[C]$.

2.2 The Metropolis Algorithm

Metropolis *et al.* [15] proposed the following choice for the probability $W[C \to C']$ for accepting the suggested configuration C',

$$W[C \to C'] = \min\{1, \exp(-\beta \Delta H)\}\,. \tag{2.5}$$

In order to accept a change with a given probability, say $W < 1$, one first generate a random number $\alpha \in [0, 1)$ which follows a uniform distribution. If $\alpha \leq W$ one accepts the change; otherwise, one retains the previous configuration.

The following algorithm describes the Monte Carlo method in a spin model using the Metropolis algorithm for a local update with a general Hamilton function $\mathcal{H}$.

Algorithm 1. Metropolis algorithm

1. Choose a spin $\vec{e}_x$ in the current configuration C.
2. Generate a trial configuration C' by performing a local transformation $\vec{e}_x \to \vec{e}\,'_x$. For the Ising model just perform the change $e_x \to -e_x$, where $e_x \in \{-1, 1\}$.
3. Calculate $\Delta\mathcal{H} = \mathcal{H}[C'] - \mathcal{H}[C]$. Accept the change $C \to C'$ with probability

$$W[C \to C'] = W[\vec{e}_x \to \vec{e}\,'_x] = \begin{cases} 1 & \text{if} \quad \Delta\mathcal{H} \leq 0 \\ \exp(-\beta\Delta\mathcal{H}) & \text{if} \quad \Delta\mathcal{H} > 0. \end{cases}$$

4. Go to step 1 using a different lattice site in order to gradually visit all the sites in the lattice.

Let us go through each step of the algorithm. Step 1 chooses a spin in the lattice, it can be a sequential or a random selection. Step 2 generates a candidate for the next configuration C' in the Markov chain. Since this is a local updating method, C and C' will just differ in the selected spin $\vec{e}_x$ or $\vec{e}\,'_x$. So going from C to C' means transforming $\vec{e}_x$ to $\vec{e}\,'_x$. In the Ising model the transformation $e_x \to e\,'_x$

is known as a "flip", since this means that a given spin $\uparrow$ will flip to $\downarrow$ and vice versa.

Step 3 refers to the physics: if the transformation decreases the energy, we will always accept the change. One may think that despite the temperature this procedure will give the system a preferred ground state, where all spins are parallel to each other, since these are the minimal energy configurations. The Metropolis algorithm prevents this from happening by giving a non-zero probability to transitions to configurations of higher energy, otherwise detailed balance does not hold. If the transformation increases the energy, we do not necessarily reject it but give it a probability of acceptance governed by the Boltzmann factor $\exp(-\beta\Delta\mathcal{H})$. Here, $\Delta\mathcal{H}$ is the energy needed to transform spin $\vec{e}_x$ to $\vec{e}\,'_x$. At low temperature the Boltzmann factor is almost zero, so the probability of transformations with $\Delta\mathcal{H} > 0$ is very small, therefore the system will prefer to be near a ground state. At high temperatures the Boltzmann factor is almost one, so the transition probability is large. Therefore the spins will point in random directions so the system is in the symmetric phase.

If we go through the lattice in a lexicographic order, step 4 ensures that we visit to all spins in the lattice. This process is known as one *sweep*. One can easily check that the Metropolis algorithm satisfies ergodicity and detailed balance [15].

Local updating methods like Metropolis suffers from a problem called *critical slowing down*, which means that near a critical point it becomes hard for the simulation to generate statistically independent configurations. To suppress critical slowing down, several methods have been applied, like cluster methods such as the Swendsen-Wang algorithm [16] and the *Wolff algorithm* [17].

2.3 The Wolff Algorithm

The Wolff algorithm is a non-local updating method that constructs sets of spins or clusters in a sophisticated way, and "flips" them according to a given transformation. It exists in a single-cluster and a multi-cluster version. Let us refer in the following algorithm to the multi-cluster version for a d-dimensional O(N) model with the standard Hamilton function, without any additional terms.

Algorithm 2. Wolff Algorithm

1. Generate a random unit vector $\vec{r} \in \mathbb{R}^N$, $|\vec{r}| = 1$, and denote its direction as the *Wolff direction*.

2. Choose a spin $\vec{e}_x$ in the current configuration C that does not belong to any existing cluster. Take $\vec{e}_x$ as the pivot to construct the cluster $\mathcal{C}_i$. Add $\vec{e}_x$ to $\mathcal{C}_i$.

3. Consider $\Delta\mathcal{H} = b' - b$, where $b = -\vec{e}_x \cdot \vec{e}_{x+\hat{\mu}}$ (here $\hat{\mu}$ is a unit vector which can take any of the $2d$ directions along the axes of the lattice: $\pm\hat{x}_1, \pm\hat{x}_2, ..., \pm\hat{x}_d$) and $b' = -\vec{e}_x \cdot \vec{e}\,'_{x+\hat{\mu}}$, where $\vec{e}\,'_x = \vec{e}_x - 2\vec{r}(\vec{r}\cdot\vec{e}_x)$ is the flipped spin. Set a *bond* between spin $\vec{e}_x$ and $\vec{e}\,'_{x+\hat{\mu}}$ with probability

$$P_{x,x+\hat{\mu}} = \begin{cases} 1 - \exp\left(-\beta\Delta\mathcal{H}\right) & \text{if} \quad \Delta\mathcal{H} > 0 \\ 0 & \text{if} \quad \Delta\mathcal{H} \leq 0. \end{cases}$$

   If the bond is accepted, then $\vec{e}_x$ and $\vec{e}_{x+\hat{\mu}}$ belong to the same cluster, and we add $\vec{e}_{x+\hat{\mu}}$ to $\mathcal{C}_i$. From $\vec{e}_x$ exhaust all other $\hat{\mu}$ directions.

4. Return to step 3 using $\vec{e}_{x+\hat{\mu}}$ (if it exists) as the pivot which already belongs to the cluster in order to set bonds with other spins. This is done until all the bonds are exhausted and the cluster is finished.

5. Return to step 2 until all the spins in the lattice belong to some cluster.

6. Collectively flip all spins in each cluster, i.e. perfrom the transformation $\vec{e}_x \to \vec{e}\,'_x$, with probability $P_{\text{flip}} = \frac{1}{2}$.

Let us go through each step. In the Ising model it is clear what we mean by a flip since this model has just two options for the spin direction. For $N \geq 2$, however, spins can point in infinitely many directions: in the XY-model spins are defined in the circumference of the unit circle S^1, in the Heisenberg model, spins live in the surface of the unit sphere S^2, in the O(4) model, spins point in the 3-d surface of a 4-dimensional unit sphere S^3, etc. We need some sort of orientation,

like we have in the Ising model to define when a spin is "up" or "down", in order to define a flip.

Step 1 generates a random vector $\vec{r}$, its direction is called the Wolff direction. This direction defines a plane that is perpendicular to $\vec{r}$, this plane is known as the *Wolff plane*[1]. We perform the flip with respect to this Wolff plane. If $\vec{r}\cdot\vec{e}_x > 0$ we say that $\vec{e}_x$ is "above" the Wolff plane (up). If $\vec{r}\cdot\vec{e}_x < 0$, then $\vec{e}_x$ is "below" (down). What we do is to flip the projection of $\vec{e}_x$ with respect to $\vec{r}$ to the other side of the Wolff plane. The resulting spin $\vec{e}\,'_x$ will be the mirror image of $\vec{e}_x$ with respect to the Wolff plane, see figure 2.1.

Step 2 selects a spin $\vec{e}_x$ in the lattice. This spin is the first one in our cluster, from this we will possibly add more spins. In step of 3 the algorithm we consider creating the bonds between all nearest neighbor spins of $\vec{e}_x$ that are all in the same half-space with respect to the Wolff plane using the complementary probability of the Boltzmann factor $1 - \exp(-\beta\Delta\mathcal{H})$. If some bonds are accepted we add these new spins to the cluster. From the accepted spins we will repeat the same procedure discarding, the spins that already belong to the cluster (step 4).

The algorithm ensures that a bond is never tried more than once. However a single spin can be tried more than once by any of the other links that connect it to the cluster. In step 5 we construct all other clusters to fill the lattice. Finally we flip each cluster with probability 1/2. Going through the whole algorithm once is in this case known as one *sweep*. For the single-cluster algorithm we always flip the constructed cluster. Also, the definition of a sweep is to perform $V/\langle\text{cluster size}\rangle$ updates of the algorithm (the cluster size is the number of spins in each cluster).

Figure 2.2 illustrates the process of accepting bonds and identifying clusters. Black points ● represent spins "up", and white circles ○ represent spins "down", bold black lines represent a bond.

[1] In $N = 2$ the Wolff plane is a line. In $N = 3$ is indeed a plane, but in $N > 3$ this is a $N - 1$ dimensional hyper-plane. Whichever the case is, we will call it indistinctly the "Wolff plane".

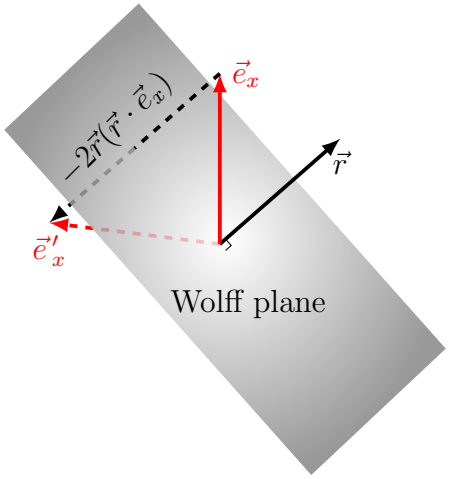

Figure 2.1: A unit vector $\vec{r}$ defines the Wolff plane. We apply the flip to $\vec{e}_x$ by taking its mirror image with respect to the Wolff plane. The flipped version of $\vec{e}_x$ is $\vec{e}\,'_x = \vec{e}_x - 2\vec{r}(\vec{r}\cdot\vec{e}_x)$, with lenght $|\vec{e}\,'_x| = |\vec{e}_x| = 1$.

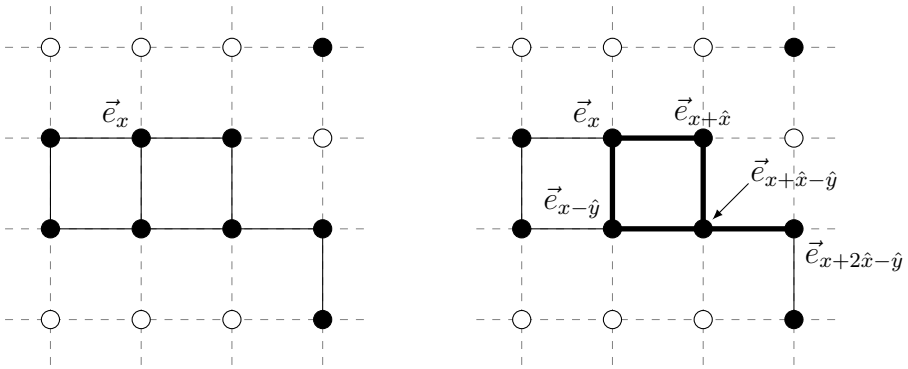

Figure 2.2: **(a)** Initial cluster with one element $\mathcal{C} = \{\vec{e}_x\}$. **(b)** Completed cluster with five elements $\mathcal{C} = \{\vec{e}_x, \vec{e}_{x+\hat{x}}, \vec{e}_{x-\hat{y}}, \vec{e}_{x+\hat{x}-\hat{y}}, \vec{e}_{x+2\hat{x}-\hat{y}}\}$.

2.4 Adding more terms to the Hamilton function

In order to take into account the contributions of extra terms in the in Hamilton function, such as an external magnetic field $\vec{h}$ or a chemical potential μ, we will modify the Wolff algorithm[2] and consider two options. The first one is to change the probability of flipping the clusters [18]. The other one is to introduce a *ghost spin* [19] that is a "neighbor" to every spin in the lattice; it changes the way clusters are created.

2.4.1 Modified flip probability

We will modify step 6 of Algorithm 2. Consider the standard form of the Hamilton function, let us call it $\mathcal{H}_0$, and add an extra term $\tilde{\mathcal{H}}$ which may include the external magnetic field and/or the chemical potential,

$$\mathcal{H}[\vec{e}] = \mathcal{H}_0 + \tilde{\mathcal{H}}$$

$$\mathcal{H}_0 = -J \sum_{\langle xy \rangle} \vec{e}_x \cdot \vec{e}_y.$$

In step 3 of Algorithm 2, the Hamilton function for creating bonds is $\mathcal{H}_0$.

Modified flip probability

6. Suggest the flip of the cluster with probability $p = 1/2$ but do not flip it. If the suggestion is accepted, then we flip the cluster with probability

$$P_{\text{flip}} = \begin{cases} 1 & \text{if } \Delta\tilde{\mathcal{H}} \leq 0 \\ \exp\left(-\beta\Delta\tilde{\mathcal{H}}\right) & \text{otherwise,} \end{cases}$$

where $\Delta\tilde{\mathcal{H}} = \tilde{\mathcal{H}}\left[C_i'\right] - \tilde{\mathcal{H}}[C]$. Here, $\tilde{\mathcal{H}}[C]$ stands for the the energy from the extra terms in the current configuration, and $\tilde{\mathcal{H}}\left[C_i'\right]$ means that only the spins in the cluster $\mathcal{C}_i$ are flipped.

[2] The Metropolis method is general and can be used for any real Hamilton function.

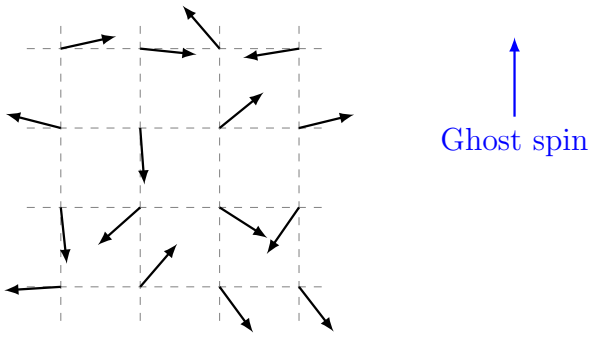

Figure 2.3: The ghost spin is considered to be a neighbor to every spin in the lattice.

2.4.2 Ghost spin

We define the ghost spin $\vec{e}_0 \in \mathbb{R}^N$ as a unit vector in the direction of the external magnetic field, $\vec{e}_0 = \frac{\vec{h}}{|\vec{h}|}$. This vector will act as a neighbor to each spin in the lattice (like a *ghost*), see figure 2.3. The following algorithm provides a procedure assuming that the extra term is only the magnetic field $\vec{h}$.

Algorithm 3. Ghost spin

1. Generate a random unit vector $\vec{r} \in \mathbb{R}^N$, $|\vec{r}| = 1$ and take its direction as the *Wolff direction*.

2. Generate bonds between $\vec{e}_0$ and the spins in the lattice with probability $1 - e^{-2h\beta(\vec{r}\cdot\vec{e}_0)(\vec{r}\cdot\vec{e}_x)}$ if $(\vec{r}\cdot\vec{e}_0)(\vec{r}\cdot\vec{e}_x) > 0$. The cluster formed with these bonds is called the *ghost cluster*.

3. Carry out the same steps to form clusters as in Algorithm 2 — other clusters can be linked to the ghost cluster — except that we do not flip the ghost cluster.

The main difference between the clusters formed with the Wolff algorithm and the ones formed with the ghost spin is that the ghost cluster can be disjoint.

In order to include other terms in the Hamilton function beside $\vec{h}$, like a chemical potential μ, carry out this algorithm but this time instead of flipping with probability 1/2 we perform the step of the modified flip probability described earlier. In this case, $\tilde{\mathcal{H}} = \mu N$, where N generally represents the particle number.

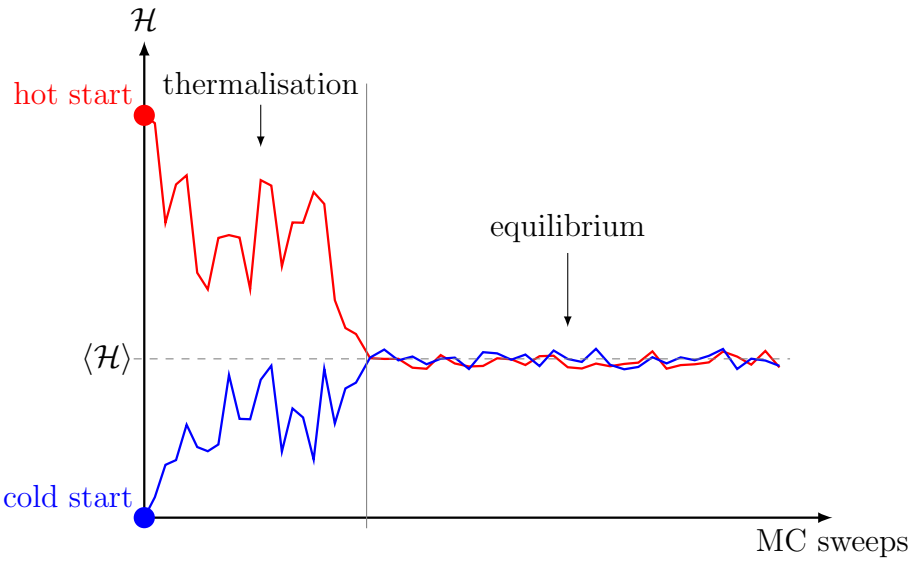

Figure 2.4: Depiction of the process to attain to thermal equilibrium as the simulation runs.

2.5 Extracting information from simulations

2.5.1 Starting points

In order to implement discrete translational invariance, we will use periodic boundary conditions. With this choice of boundaries, every site in the lattice is equivalent to any other. It is the most popular choice for boundary conditions.

To start a simulation we need some initial configuration C_0. If we generate C_0 such that the spins point in random directions, we say that C_0 is a *hot start*. If instead C_0 is one of the vacuum configurations where spins are parallel, we call it a *cold start*. Usually none of these two starts represents a preferred configuration of the system, therefore, we let the system reach equilibrium after a number N_{therm} of Monte Carlo sweeps. This process of reaching equilibrium is known as *thermalisation*. Figure 2.4 illustrates this process.

2.5.2 Taking measurements

We will discard all the sweeps of thermalisation before data collection in order to attain thermal averages without systematic errors inherited from the non-equilibrium configurations. To obtain statistically independent configurations, we

skip a number N_{skip} of sweeps between the measurements. Now we are ready to compute all the thermal averages of quantities of interest. Let us summarize what we have to do: a depiction of

1. Generate C_0 (hot or cold start).
2. Perform N_{therm} configurations.
3. Take measurements every N_{skip} sweeps after thermalisation.
4. End the simulation after taking N_{meas} measurements.
5. Compute thermal averages and their statistical errors.

As they stand, the definitions for the magnetization density (1.21) and the magnetic susceptibility (1.22) are not useful if we simulate a finite system. This is because $\langle \vec{M} \rangle$ is zero at $h = 0$, since the average over all configurations must vanish. As such, averaging only the magnetization would yield incorrect results. To overcome this problem we take the average of the absolute value of the magnetization as pointed out in Ref. [20]. Thus now we arrive to new definitions of these quantities,

$$\text{magnetization density } m = \frac{1}{V}\langle |\vec{M}| \rangle \tag{2.6}$$

$$\text{magnetic susceptibility } \chi_m = \frac{\beta}{V}\left(\langle \vec{M}^2 \rangle - \langle |\vec{M}| \rangle^2 \right) . \tag{2.7}$$

2.6 The sign problem

The sign problem refers to the difficulty of computing the integral of a rapidly oscillating function. For instance, if we try to compute the expectation value of a quantity $O[C]$ weighted with $e^{-S_0[C]+i\mu N[C]}$

$$\langle O \rangle = \frac{\int \mathcal{D}C\, O[C] e^{-S_0[C]+i\mu N[C]}}{\int \mathcal{D}C\, e^{-S_0[C]+i\mu N[C]}},$$

where S_0, μ, $N \in \mathbb{R}$, we realize that it is impossible to evaluate this expression by generating configurations weighted by $p[C] \propto e^{-S_0[C]+i\mu N[C]}$. This is because the weight function is now a complex number and cannot be interpreted as a probability anymore.

In the context of QCD, the sign problem has prevented conclusive numerical simulations at high baryonic chemical potential to explore the QCD phase diagram.

An attempt to deal with this problem is to generate the configurations weighted with the real part $\exp(-S_0)$, and let the observable O absorb the imaginary part $\exp(i\mu N)$. This process is called *reweighting*. Unfortunately, due to the rapid oscillations, one needs an exponentially large statistichs as the volume of the system grows. For a general overview on this topic we refer to Ref. [21].

In this thesis we will circumvent the sign problem by studying an effective model that does not suffer from it.

Chapter 3

Quantum Chromodynamics and Chiral Perturbation Theory

3.1 Quantum Chromodynamics (QCD)

From now on we will work with the Euclidean time functional integral formalism. As we described in Chapter 1, QCD is the $SU(3)$ part of the Standard Model that describes the strong interaction of (colored) quarks and gluons. In the pure QCD sector, the left-hand and right-hand chiral $SU(2)$ quark doublets — in the next section we give the definitions of left and right handedness —

$$\begin{pmatrix} u_{L,R}(x) \\ d_{L,R}(x) \end{pmatrix}, \begin{pmatrix} c_{L,R}(x) \\ s_{L,R}(x) \end{pmatrix}, \begin{pmatrix} t_{L,R}(x) \\ b_{L,R}(x) \end{pmatrix},$$

couple in the same way to the gluon field. Hence the mass term can be written into the QCD Lagrangian without gauge symmetry breaking as follows

$$\begin{aligned} \mathcal{L}_{\mathrm{QCD}}(\bar{\Psi}, \Psi, G_\mu) = & \sum_{\mathrm{f}} \bar{\Psi}_{\mathrm{f,L}}(x) \left(i\gamma_\mu[\partial_\mu + g_{\mathrm{s}} G_\mu(x)]\right) \Psi_{\mathrm{f,L}}(x) \\ & + \sum_{\mathrm{f}} \bar{\Psi}_{\mathrm{f,R}}(x) \left(i\gamma_\mu[\partial_\mu + g_{\mathrm{s}} G_\mu(x)]\right) \Psi_{\mathrm{f,R}}(x) \\ & + \sum_{\mathrm{f}} m_{\mathrm{f}} \left(\bar{\Psi}_{\mathrm{fL}}(x)\Psi_{\mathrm{fR}}(x) + \bar{\Psi}_{\mathrm{fR}}(x)\Psi_{\mathrm{fL}}(x)\right) \\ & + \frac{1}{4}\mathrm{Tr}\left[G_{\mu\nu}(x)G_{\mu\nu}(x)\right], \end{aligned} \tag{3.1}$$

where repeated indices are summed over. The γ_μ are the Dirac matrices. The spinor fields $\Psi_\mathrm{f} = \Psi_{\mathrm{f,L}} + \Psi_{\mathrm{f,R}}$ represent a quark of flavor $\mathrm{f} \in \{u, d, \ldots, t\}$ and mass m_f. The gluons are introduced through an algebra-valued gauge potential $G_\mu(x) = iG^a_\mu\lambda_a$, $a \in \{1, 2, \ldots, 8\}$, where λ_a are eight 3×3 matrices and are the generators of the $SU(3)$ color group such that $\lambda_a^\dagger = \lambda_a$, $\mathrm{Tr}\lambda_a = 0$. Now we choose a representation of λ_a, let us take the *Gell-Mann matrices*,

$$\lambda_1 = \begin{pmatrix} 0 & 1 & 0 \\ 1 & 0 & 0 \\ 0 & 0 & 0 \end{pmatrix} \ , \ \lambda_2 = \begin{pmatrix} 0 & -i & 0 \\ i & 0 & 0 \\ 0 & 0 & 0 \end{pmatrix} \ , \ \lambda_3 = \begin{pmatrix} 1 & 0 & 0 \\ 0 & -1 & 0 \\ 0 & 0 & 0 \end{pmatrix}$$

$$\lambda_4 = \begin{pmatrix} 0 & 0 & 1 \\ 0 & 0 & 0 \\ 1 & 0 & 0 \end{pmatrix} \ , \ \lambda_5 = \begin{pmatrix} 0 & 0 & -i \\ 0 & 0 & 0 \\ i & 0 & 0 \end{pmatrix} \ , \ \lambda_6 = \begin{pmatrix} 0 & 0 & 0 \\ 0 & 0 & 1 \\ 0 & 1 & 0 \end{pmatrix}$$

$$\lambda_7 = \begin{pmatrix} 0 & 0 & 0 \\ 0 & 0 & -i \\ 0 & i & 0 \end{pmatrix} \ , \ \lambda_8 = \frac{1}{\sqrt{3}} \begin{pmatrix} 1 & 0 & 0 \\ 0 & 1 & 0 \\ 0 & 0 & -2 \end{pmatrix} \ , \tag{3.2}$$

this representation ensures the normalization relation

$$\mathrm{Tr}(\lambda_a\lambda_b) = 2\delta_{ab}. \tag{3.3}$$

The gluon field strength tensor $G_{\mu\nu}$ is given by

$$\begin{aligned} D_\mu &= \partial_\mu + g_\mathrm{s}G_\mu \\ G_{\mu\nu} &= \frac{1}{g_\mathrm{s}}[D_\mu, D_\nu] = \partial_\mu G_\nu - \partial_\nu G_\mu + g_\mathrm{s}[G_\mu, G_\nu], \end{aligned} \tag{3.4}$$

where g_s is the dimensionless gauge coupling constant of the strong interaction.

3.2 Chiral symmetry in QCD

We introduce the Euclidean chirality matrix $\gamma_5 = \gamma_1\gamma_2\gamma_3\gamma_4$, $\gamma_5^2 = \mathbb{1}$, $\{\gamma_5, \gamma_\mu\} = 0$, and define the projection operators

$$P_\pm = \frac{1}{2}(1 \pm \gamma_5)\,. \tag{3.5}$$

Now defining left-handed and right-handed fermions

$$\psi_{L,R} = P_\mp \psi,\ \bar{\psi}_{L,R} = \bar{\psi} P_\pm\,, \tag{3.6}$$

we can rewrite the QCD Lagrangian (3.1) considering the chiral limit — i.e. massless quarks — as follows

$$\mathcal{L}_{\mathrm{QCD}} = \sum_{\mathrm{f}} \left(\bar{\psi}_{\mathrm{L,f}} i \not{D} \psi_{\mathrm{L,f}} + \bar{\psi}_{\mathrm{R,f}} i \not{D} \psi_{\mathrm{R,f}}\right) + \frac{1}{4}\mathrm{Tr}\left[G_{\mu\nu} G_{\mu\nu}\right]\,, \tag{3.7}$$

where $\not{D} = \gamma_\mu D_\mu$. We see that (3.7) reveals that the QCD Lagrangian has a global symmetry $U(N_f)_{\mathrm{L}} \otimes U(N_f)_{\mathrm{R}}$ under separate $U(N_f)$ transformations of the left-handed and right-handed quarks for N_f massless quark flavors. We can decompose each $U(N_f)$ symmetry into a $SU(N_f)$ and a $U(1)$ part, hence we obtain

$$SU(N_f)_{\mathrm{L}} \otimes SU(N_f)_{\mathrm{R}} \otimes U(1)_{\mathrm{B}} \otimes U(1)_{\mathrm{A}}\,. \tag{3.8}$$

Under the $U(1)_{\mathrm{B}}$ symmetry, both the left and right handed fermions transform in the same way: $\psi_{R,L} \to e^{i\alpha}\psi_{R,L}$. Its conserved associated charge corresponds to the baryon number.

The $U(1)_{\mathrm{A}}$ is anomalous and it is explicitly broken by the *Adler-Bell-Jackiw anomaly*. Under this symmetry, both the left-handed and right-handed fermions transform with opposite phase: $\psi_{R,L} \to e^{\pm i\alpha}\psi_{R,L}$. The remaining chiral flavor symmetry breaks spontaneously

$$SU(N_f)_{\mathrm{L}} \otimes SU(N_f)_{\mathrm{R}} \to SU(N_f)_{\mathrm{L=R}}\,, \tag{3.9}$$

which, according to the Goldstone theorem [22, 23] gives rise to $N_f^2 - 1$ NGBs.

An important order parameter for the chiral SSB in QCD is the *chiral condensate*

$$\Sigma \equiv -\langle \bar{\Psi}_{\mathrm{f}} \Psi_{\mathrm{f}} \rangle = -\langle 0 | \bar{\Psi}_{\mathrm{f}}(x) \Psi(x)_{\mathrm{f}} | 0 \rangle \,, \tag{3.10}$$

where sum over the index f is implicit. Σ is a measure of the density of quark-antiquark pairs that have condensed into the same quantum state. It is expected to vanish at high temperatures, so the system is in the chiral phase. Numerical QCD analysis reveals a value $\Sigma \approx (250\,\mathrm{MeV})^3$.

3.3 Chiral perturbation theory

At low energies some field theories can be described by an *effective field theory*, which is an approximation of the more fundamental theory.

If we consider QCD at low energies, compared with its intrinsic scale Λ_{QCD}, the first generation of quarks dominates nuclear physics. The effective theory of QCD is known as *Chiral Perturbation Theory* (ChPT), which instead of taking the quarks and gluons as the fundamental degrees of freedom, takes the Nambu-Goldstone bosons which manifest at low energies after the spontaneous symmetry breaking of the chiral symmetry. The parameters that ChPT involves are the so-called *low energy coupling constants* [24, 25, 26].

Considering massless quarks, the two flavor QCD Lagrangian has a global symmetry $G = SU(2)_{\mathrm{L}} \otimes SU(2)_{\mathrm{R}} \simeq \mathrm{O}(4)$ with $n_G = 3 + 3 = 6$ generators, which then spontaneously breaks down to $H = SU(2)_{L=R} \simeq \mathrm{O}(3)$ with $n_H = 3$ generators. According to Goldstone's theorem this gives rise to $n_G - n_H = 6 - 3 = 3$ massless NGBs. ChPT describes the NBGs by fields in the coset space $G/H = SU(2) \simeq \mathrm{O}(3)$. In QCD we identify these three NGBs to the three pions π^0, π^+, π^-. If we consider instead three flavors, these quasi NGBs are the light meson octet, consisting of the three pions, the four kaons and the η-meson.

In this sense our fields need to take the form of 2×2 matrices $U(x) \in SU(2)$.

An element of $SU(2)$ can be written in the following matrix form

$$U = \begin{pmatrix} z_1 & -z_2^* \\ z_2 & z_1^* \end{pmatrix}, \; U^\dagger U = 1\,, \tag{3.11}$$

where $z_1\,, z_2 \in \mathbb{C}$, with $\det U = |z_1|^2 + |z_2|^2 = 1$. Since the matrix $U(x)$ is described by two complex numbers, and therefore four real numbers, we can also describe an element of $SU(2)$ with a real four component vector $\vec{e}(x) \in \mathbb{R}^4$ with $|\vec{e}(x)| = 1$. In other words, the $SU(2)$ group is isomorphic to the 3 dimensional sphere S^3, and therefore $\vec{e}(x) \in S^3$.

What form should the Lagrangian of our effective theory take? In ChPT it is enough to describe the system with fields in the coset space. However, we also want to take into account the chiral symmetry and the SSB exhibited by the system, so we need a Lagrangian that is $SU(2)_{\mathrm{L}} \otimes SU(2)_{\mathrm{R}} \simeq O(4)$ invariant, and which can break down to $SU(2)_{\mathrm{L=R}} \simeq \mathrm{O}(3)$.

3.3.1 The non-linear σ-model

Since we want a Lagrangrian which is compatible with the idea of low energies, we have to construct one with the least number of derivatives, since this represents the power of momenta,

$$\mathcal{L}_{\mathrm{kin}}(U) = \frac{F_\pi^2}{4} \mathrm{Tr}\left[\partial_\mu U^\dagger \partial_\mu U\right], \; U(x) \in SU(2), \tag{3.12}$$

where $F_\pi \approx 92.4\,\mathrm{MeV}$ is the low energy constant, known as the *pion decay constant*. Regarding chiral flavor symmetry, the field $U(x)$ transforms as

$$U(x) \to U'(x) = LU(x)R^\dagger, \; \partial_\mu U(x) \to \partial_\mu U'(x) = L\partial_\mu U(x) R^\dagger \tag{3.13}$$

where $L \in SU(2)_L$ and $R \in SU(2)_R$, and therefore

$$\mathcal{L}_{\mathrm{kin}}(U') = \frac{F_\pi^2}{4} \mathrm{Tr}\left[\partial_\mu U'^\dagger \partial_\mu U'\right] = \frac{F_\pi^2}{4} \mathrm{Tr}\left[R\partial_\mu U^\dagger L^\dagger L \partial_\mu U R^\dagger\right] = \mathcal{L}_{\mathrm{kin}}(U). \tag{3.14}$$

The last equality is due to the fact that $L^\dagger L = R^\dagger R = \mathbb{1}$, along with the cyclic property of the trace.

Alternatively, the Lagrangian can be formulated with the field $\vec{e}(x)$,

$$\mathcal{L}_{\text{kin}}(\vec{e}) = \frac{F_\pi^2}{2}\partial_\mu \vec{e}^{\,T}\partial_\mu \vec{e}. \tag{3.15}$$

The field $\vec{e}(x)$ transforms with elements $\mathcal{O} \in O(4)$ as

$$\vec{e}(x) \to \vec{e}(x)' = \mathcal{O}\vec{e}(x)\,,\ \partial_\mu \vec{e}(x) \to \partial_\mu \vec{e}(x)' = \mathcal{O}\partial_\mu \vec{e}(x)\,, \tag{3.16}$$

and therefore

$$\mathcal{L}_{\text{kin}}(\vec{e}\,') = \frac{F_\pi^2}{2}\partial_\mu \vec{e}^{\,\prime\,T}\partial_\mu \vec{e}\,' = \frac{F_\pi^2}{2}\partial_\mu \vec{e}^{\,\prime\,T}\mathcal{O}^T\mathcal{O}\partial_\mu \vec{e}\,' = \mathcal{L}_{\text{kin}}(\vec{e})\,, \tag{3.17}$$

since $\mathcal{O}^T\mathcal{O} = \mathbb{1}$. In summary, the Lagrangian (3.15) is invariant under O(4) transformations, and the field $\vec{e}(x)$ has a non-linear constrain $|\vec{e}(x)| = 1$. Therefore the system is described by the non-linear σ-model [4] that we described in Section 1.2.

3.4 The inclusion of quark masses

In reality the chiral symmetry is only approximate, since quarks are massive, therefore the chiral symmetry is explicitly broken. This provides the NGBs with a small non-zero mass. Nevertheless, ChPT is still applicable in the massive quark case.

We know that the chiral symmetry breaking term in the Lagrangian of QCD is of the form

$$\mathcal{L}_m = \sum_{\text{f}} m_{\text{f}} \left(\bar{\Psi}_{\text{fL}}(x)\Psi_{\text{fR}}(x) + \bar{\Psi}_{\text{fR}}(x)\Psi_{\text{fL}}(x)\right). \tag{3.18}$$

In our effective theory, we have to map this term onto another one which breaks

the symmetry in the same way,

$$\mathcal{L}_{m,\text{eff}}(U) = c_1 \text{Tr}[\mathcal{M}(U + U^\dagger)]\,, \tag{3.19}$$

where $\mathcal{M} = \text{diag}(m_u, m_d, \dots)$, and transforms as

$$\mathcal{L}_{m,\text{eff}}(U') = c_1 \text{Tr}[\mathcal{M}(U' + U'^\dagger)] = c_1 \text{Tr}[\mathcal{M}(LUR^\dagger + RU^\dagger L^\dagger)]\,. \tag{3.20}$$

For quark flavors with equal masses, $\mathcal{M} = m_q \mathbb{1}$, we obtain

$$\mathcal{L}_{m,\text{eff}}(U) = c_1 m_q \text{Tr}[(U + U^\dagger)]\,, \tag{3.21}$$

which is symmetric under $SU(N_\text{f})_{L=R}$ transformations.

Now we have to determine the value of the low energy constant c_1. As such, we first have to obtain the vacuum expectation value of $(\partial/\partial m_\text{f})\mathcal{L}_\text{QCD}|_{\mathcal{M}=0}$

$$\langle 0|\frac{\partial}{\partial_{m_\text{f}}}\mathcal{L}_\text{QCD}|_{\mathcal{M}=0}|0\rangle = \langle 0|\bar{\Psi}_\text{f}\Psi_\text{f}|0\rangle = -\frac{1}{N_\text{f}}\langle(-\bar{\Psi}\Psi)\rangle = -\frac{1}{N_\text{f}}\Sigma\,. \tag{3.22}$$

The same value should arise when taking the vacuum value of our effective Lagrangian. The classical solution corresponds to a constant field $U(x) = \mathbb{1}$,

$$\langle 0|\frac{\partial}{\partial_{m_\text{f}}}\mathcal{L}_{m,\text{eff}}|_{\mathcal{M}=0}|0\rangle = c_1 \text{Tr}[\text{diag}(0, ..., 0, 1, 0, ..., 0)(\mathbb{1} + \mathbb{1})] = 2c_1\,, \tag{3.23}$$

and therefore,

$$c_1 = -\frac{1}{2N_\text{f}}\Sigma\,. \tag{3.24}$$

Hence, the complete Lagrangian with two quark flavors with equal masses takes the form

$$\mathcal{L}_\text{eff}(U) = \frac{F_\pi^2}{4}\text{Tr}\left[\partial_\mu U^\dagger \partial_\mu U\right] - \frac{1}{4}\Sigma\,\text{Tr}[\mathcal{M}(U + U^\dagger)]\,. \tag{3.25}$$

Using the field $\vec{e}(x)$, the effective Lagrangian for $N_\text{f} = 2$ is of the form

$$\mathcal{L}_\text{eff}(\vec{e}) = \frac{F_\pi^2}{2}\partial_\mu \vec{e}^{\,T}\partial_\mu \vec{e} - \vec{h}\cdot\vec{e}\,. \tag{3.26}$$

The second term breaks explicitly the O(4) symmetry down to O(3), so it also

follows the same symmetry breaking pattern as $\mathcal{L}_{\text{QCD}}$. The low energy constant in this term can be perfectly included in the definition of the external field $\vec{h}$.

3.4.1 Masses of quasi-NBGs

In order to obtain the masses of the quasi-NGBs we are going to expand around the vacuum solution $U(x) = \mathbb{1}$. We write $U(x) = \exp(i\pi_a(x)\eta_a/F_\pi)$, where $a = 1, 2, \ldots, N_f^2 - 1$, η_a are the generators of $SU(N_f)$, normalized such that $\text{Tr}[\eta_a\eta_b] = 2\delta_{a,b}$ generalizing equation (3.3). Now we expand consistently in powers of the quasi-NBGs up to order $\pi_a(x)^2$

$$U(x) = \mathbb{1} + i\pi_a(x)\eta_a/F_\pi - \frac{1}{2}(\pi_a(x)\eta_a/F_\pi)^2\,. \tag{3.27}$$

Considering equal quark masses, $\mathcal{M} = m_q\mathbb{1}$, the mass term of the effective Lagrangian is

$$\begin{aligned}\text{Tr}[\mathcal{M}(U + U^\dagger)] &= m_q\,\text{Tr}[U + U^\dagger] \\ &= 2m_qN_f - m_q\frac{1}{F_\pi^2}\pi_a(x)\pi_b(x)\,\text{Tr}[\eta_a\eta_b] \\ &= 2m_q\left(N_f - \frac{1}{F_\pi^2}\pi_a(x)\pi_a(x)\right)\,.\end{aligned} \tag{3.28}$$

Together with the kinetic we obtain

$$\mathcal{L}_{\text{eff}} = \frac{1}{2}\partial_\mu\pi_a\partial_\mu\pi_a - \frac{m_q}{N_f}\Sigma\left(N_f - \frac{1}{F_\pi^2}\pi_a(x)\pi_a(x)\right)\,. \tag{3.29}$$

In classical field theory the corresponding equation of motion is given by

$$\partial_\mu\frac{\delta\mathcal{L}_{\text{eff}}}{\delta\partial_\mu\pi_a} - \frac{\delta\mathcal{L}_{\text{eff}}}{\delta\pi_a} = \partial_\mu\partial_\mu\pi_a - \frac{2m_q\Sigma}{N_fF_\pi^2}\pi_a = 0\,. \tag{3.30}$$

This is the Klein-Gordon equation in Euclidean time, for a pseudo-scalar particle π_a with mass M_π,

$$M_\pi^2 = \frac{2m_q\Sigma}{N_fF_\pi^2}\,. \tag{3.31}$$

This expression is known as the *Gell-Mann–Oakes–Renner* relation [27].

Considering again two quark flavors we have

$$M_\pi^2 = \frac{m_q \Sigma}{F_\pi^2} \,. \tag{3.32}$$

It is natural to relate $h \sim m_q \Sigma$.

3.5 Dimensional reduction

Let us consider the system in a finite volume. We assume periodic boundary conditions, as we mentioned in Chapter 2, this provides translation invariance.

Since we are working with four spacetime dimensions, we assume a 4-d volume of the form $\beta \times V$, where β is the extent in Euclidean time t_E, and V is the 3-d spatial volume of a cube of length L. Therefore the Euclidean action for our effective model reads

$$S_\mathrm{E}[\vec{e}] = \int_0^\beta dt_\mathrm{E} \int_V d^3x \left(\frac{F_\pi^2}{2} \partial_\mu \vec{e}(x) \cdot \partial_\mu \vec{e}(x) - \vec{h} \cdot \vec{e}(x) \right) . \tag{3.33}$$

We are going to consider the case of short β, which in field theory corresponds to $\beta = 1/T$, therefore we consider the case of high temperature. In this case only the leading modes contribute significantly. All other modes have a higher energy, $p = 2\pi n/\beta$, $n \in \mathbb{Z}$, so in our low effective theory those modes decouple. This indicates that the Lagrangian is almost constant in t_E, and the action (3.33) reduces to

$$S_\mathrm{E}[\vec{e}] = \beta \int_V d^3x \left(\frac{F_\pi^2}{2} \partial_i \vec{e}(x) \cdot \partial_i \vec{e}(x) - \vec{h} \cdot \vec{e}(x) \right) , \tag{3.34}$$

where $i = 1, 2, 3$ in contrast to $\mu = 1, 2, 3, 4$. This simplification is known as *dimensional reduction*. The dimensional reduction takes us to the 3-d $O(4)$ model, which is endowed with topological charges.

3.6 The inclusion of the baryonic chemical potential

At fixed Euclidean time t_{E}, the field $U(x) \in SU(2)$ maps the 3-d coordinate space into S^3. Geometry tells us that $\Pi_3[S^3] = \mathbb{Z}$ which implies that the field configurations fall into topological sectors labeled by a topological charge $Q \in \mathbb{Z}$. In this case it is given by

$$Q = \frac{1}{24\pi^2} \int d^3x \, \epsilon_{ijk} \, \mathrm{Tr} \left((U\partial_i U)(U\partial_j U)(U\partial_k U) \right) \, , i,j,k \in \{1,2,3\} \, . \tag{3.35}$$

As Skyrme pointed out [28], the topological charge can be interpreted as the baryon number, even though the field U represents mesons. This term enters in our effective theory, multiplied by the chemical potential μ_B

$$H[\vec{e}] = \int_V d^3x \left(\frac{F_\pi^2}{2} \partial_\mu \vec{e}(x) \cdot \partial_\mu \vec{e}(x) - \vec{h} \cdot \vec{e}(x) \right) - \mu_B Q[\vec{e}] \, . \tag{3.36}$$

Since Q is a dimensionless number, μ_B has dimension [mass]. It is interpreted as the energy decrease if we add a baryon, or the energy increase if we remove an anti-baryon from the system.

3.7 Lattice regularization

The functional integral as it stands is still a highly divergent expression which is undefined until we use a regularization scheme. Since we are working with the topological charge which at a perturbative level is not manifested, we need a non-perturbative approach. To this end, the only non-perturbative regularization scheme is practically the *lattice regularization*, which is perfect if we want to simulate the system with a computer.

On the lattice, the continuum field $\vec{e}(x)$ is replaced by a lattice field $\vec{e}_x$, which is defined in the sites x of the 3-d lattice, with lattice spacing a and $x/a \in \mathbb{Z}^3$.

We discretize the derivative in the standard form

$$\partial_i \vec{e}(x) \to \frac{\vec{e}_{x+a\hat{\imath}} - \vec{e}_x}{a}\,, \tag{3.37}$$

where $\hat{\imath}$ is a unit vector in the direction of the component x_i. Therefore we obtain

$$\begin{aligned}\partial_i \vec{e}(x) \cdot \partial_i \vec{e}(x) \to \sum_i \left(\frac{\vec{e}_{x+a\hat{\imath}} - \vec{e}_x}{a}\right)^2 &= \sum_i \frac{\vec{e}^{\,2}_{x+a\hat{\imath}} - 2\vec{e}_{x+a\hat{\imath}} \cdot \vec{e}_x + \vec{e}^{\,2}_x}{a^2} \\ &= \frac{2}{a^2}\sum_i (1 - \vec{e}_{x+a\hat{\imath}} \cdot \vec{e}_x)\,. \end{aligned} \tag{3.38}$$

Since we are only interested in energy differences, we can drop the additive constant. Therefore the lattice Hamiltonian is written as (with $\int d^3x \to a^3 \sum_x$)

$$H_{\rm lat}[\vec{e}] = -F_\pi^2 a \sum_x \sum_i \vec{e}_{x+a\hat{\imath}} \cdot \vec{e}_x - \mu_B Q[\vec{e}] - a^3 \vec{h} \cdot \sum_x \vec{e}_x\,. \tag{3.39}$$

We denote the inverse coupling that we will use in the simulation as $\beta_{\rm lat}$, then the lattice action reads

$$S_{\rm E,lat}[\vec{e}] = \beta_{\rm lat} H_{\rm lat}[\vec{e}] = \beta_{\rm lat}\left(-\sum_x \sum_i \vec{e}_{x+a\hat{\imath}} \cdot \vec{e}_x - \mu_{B,\rm lat} Q[\vec{e}] - \vec{h}_{\rm lat} \cdot \sum_x \vec{e}_x\right). \tag{3.40}$$

We recognize the physical meaning of the dimensionless parameters that we are inserting in the simulation code,

$$\beta_{\rm lat} = \beta F_\pi^2 a\ ,\ \mu_{B,\rm lat} = \frac{\mu_B}{F_\pi^2 a}\ ,\ h_{\rm lat} = \frac{h a^2}{F_\pi^2}\,. \tag{3.41}$$

If we consider massless quarks, simulations show that the critical value β_c when $\mu_B = 0$, where the second order phase transition takes place, is $\beta_{c,\rm lat} = 1/T_{c,\rm lat} = 0.93590$, according to Ref. [29, 30]. If we identify this critical value $\beta_{c,\rm lat}$ with the actual cross-over temperature $T_x \approx 155\,\text{MeV}$ [31], we could in principle use the ratio $\beta_x/\beta_{c,\rm lat}$ to convert $\mu_{B,\rm lat}$ and $h_{\rm lat}$ into physical units.

We need to estimate a value for $h_{\rm lat}$ that is realistic, since this term represents the mass term of the quarks. From the Gell-Mann–Oakes–Renner relation we know that h has units of $[\text{mass}]^4$, then we are going to use use the proper powers

of $\beta_x/\beta_{c,\mathrm{latt}}$ to convert it into lattice units

$$h_{\mathrm{lat}} = h\frac{\beta_x^4}{\beta_{c,\mathrm{lat}}^4} = h(145.1\,\mathrm{MeV})^{-4}\,. \tag{3.42}$$

According to the Gell-Mann–Oakes–Renner relation

$$h = F_\pi^2 M_\pi^2 \approx (92.4\,\mathrm{MeV})^2(138\,\mathrm{MeV})^2 = (112.9\,\mathrm{MeV})^4 = 1.626\times 10^8\,\mathrm{MeV}^4\,.$$

(Since we are not dealing with electromagnetic interactions, we use an intermediate value for the pion using the masses of the charged and neutral pions $M_\pi^0 \simeq 135\,\mathrm{MeV}$, $M_\pi^\pm \simeq 140\,\mathrm{MeV}$.) Inserting this into (3.42) we obtain

$$h_{\mathrm{lat}} \approx 0.367\,. \tag{3.43}$$

This value corresponds to a quark mass of

$$m_q = \frac{F_\pi^2 M_\pi^2}{\Sigma} = \frac{1.626\times 10^8\,\mathrm{MeV}^4}{(250\,\mathrm{MeV})^3} \approx 10.4\,\mathrm{MeV}\,. \tag{3.44}$$

This mass is somewhat higher than $m_u \simeq 2.2\,\mathrm{MeV}$, $m_d \simeq 4.7\,\mathrm{MeV}$, but we know that they are renormalized. However, it is in the same order of magnitude. Our SSB picture refers to the pions as the physical degrees of freedom, therefore M_π is the reliable quantity to set the scale since it is directly measurable, in contrast to the quark masses.

In conclusion, in this work we study the low energy dynamics of quasi NGBs, with two quark flavors, up and down, considering their masses as degenerate. To this end, we use the 3-d O(4) model as an effective theory. We are going to monitor the temperature $T = 1/\beta$ where the crossover takes place, in order to explore the QCD phase diagram with two massive quark flavors at finite baryon density. This is done numerically using the algorithm for O(N) models described in Chapter 2, thus avoiding the numerical sign problem [32, 33].

Chapter 4

Results for the 3-d O(4) Model

4.1 Set-up

We present simulation results for the 3-d O(4) model, obtained with the Wolff multi-cluster algorithm using a cubic lattice structure with a volume $V = L^3$, and periodic boundary conditions in all directions, with an external magnetic field, $h_{\rm lat} = |\vec{h}_{\rm lat}| = 0.367$, and with chemical potentials $\mu_{B,{\rm lat}} \in \{0, 0.2, 0.4, \ldots, 2\}$.

A spin variable is denoted as $\vec{e}_x$, with $|\vec{e}_x| = 1$, $\forall x = (x_1, x_2, x_3)$, and the standard lattice action and Hamilton function with a chemical potential μ_B and external field $\vec{h}$ are used,

$$S_{\rm lat}[\vec{e}] = \beta_{\rm lat}\mathcal{H}[\vec{e}],\ \mathcal{H}[\vec{e}] = \mathcal{H}_0 + \mathcal{H}_1 + \mathcal{H}_2 = -\sum_{\langle xy\rangle} \vec{e}_x \cdot \vec{e}_y - \vec{h}_{\rm lat} \cdot \sum_x \vec{e}_x - \mu_{B,{\rm lat}} Q[\vec{e}] \tag{4.1}$$

$$\begin{aligned} \mathcal{H}_0 &= -\textstyle\sum_{\langle xy\rangle} \vec{e}_x \cdot \vec{e}_y \\ \mathcal{H}_1 &= -\vec{h}_{\rm lat} \cdot \textstyle\sum_x \vec{e}_x \\ \mathcal{H}_2 &= -\mu_{B,{\rm lat}} Q[\vec{e}], \end{aligned}$$

where $Q[\vec{e}]$ is the topological charge. The following definitions were used to measure a set of observables:

$$\text{energy density } \epsilon = \frac{1}{V}\langle \mathcal{H} \rangle \tag{4.2}$$

$$\text{specific heat } c_v = \frac{\beta_{\text{lat}}^2}{V}\left(\langle \mathcal{H}^2 \rangle - \langle \mathcal{H} \rangle^2\right) \tag{4.3}$$

$$\text{magnetization density } m = \frac{1}{V}\langle |\vec{M}| \rangle,\ \vec{M} = \sum_x \vec{e}_x \tag{4.4}$$

$$\text{magnetic susceptibility } \chi_m = \frac{\beta_{\text{lat}}}{V}\left(\langle \vec{M}^2 \rangle - \langle |\vec{M}| \rangle^2\right) \tag{4.5}$$

$$\text{topological charge density } q = \frac{1}{V}\langle Q \rangle \tag{4.6}$$

$$\text{topological susceptibility } \chi_t = \frac{1}{V}\left(\langle Q^2 \rangle - \langle Q \rangle^2\right) \tag{4.7}$$

$$\text{time-layer connected correlator } C(r) = \langle \vec{s}_{x_3} \cdot \vec{s}_{x_3+r} \rangle - \langle \vec{s}_{x_3} \rangle \cdot \langle \vec{s}_{x_3+r} \rangle \tag{4.8}$$

$$\vec{s}_{x_3} = \frac{1}{L^2}\sum_{x_1,x_2} \vec{e}_{(x_1,x_2,x_3)}$$

Since we are dealing with periodic boundaries, the correlation length ξ is obtained from the correlation function by a 2-parameter fit to

$$C(r) = A\cosh((r - L/2)/\xi). \tag{4.9}$$

4.1.1 Topological charge

In order to compute the topological charge we first need to split the whole lattice into unit cubes, in each of these vertices lives a spin variable $\vec{e}_x$, we also split each cube into six tetrahedra with the following configuration of vertices: {F,H,A,E}, {G,B,F,H}, {H,A,B,F}, {H,G,B,D}, {A,B,D,H} and {G,B,D,C}, see figure 4.1. The four spin variables $\{\vec{e}_1, \vec{e}_2, \vec{e}_3, \vec{e}_4\}$ that live at the vertices of each of these six tetrahedra, span by themselves a spherical tetrahedron,4 see figure 4.2. Its volume will contribute to the total topological charge of the lattice. We define the topological charge as the number of times all the tetrahedra in the lattice cover the surface of the sphere S^3. It is important to mention that we take the spherical tetrahedra with minimal volume, and the contribution to Q is the oriented volume, which can be positive or negative.

The analytical formula to compute the volume of a spherical tetrahedra was

developed by Murakami in Ref. [34].

In terms of the edge lenghts l_1, l_2, l_3, l_4, l_5, l_6 of a tetrahedron T, its volume is given by

$$\begin{aligned}\mathrm{Vol}(T) =&\mathrm{Re}\left(\tilde{L}(b_1,b_2,\ldots,b_6,\tilde{z}_0)\right) - \pi\arg(-\tilde{q}_2) - \sum_{j=1}^{6} l_j \left.\frac{\partial \mathrm{Re}\left(\tilde{L}(b_1,b_2,\ldots,b_6,z)\right)}{\partial l_j}\right|_{z=\tilde{z}_0} \\ &- \frac{1}{2}\pi^2 \mod 2\pi^2, \end{aligned} \tag{4.10}$$

where we define $b_j = e^{il_j}$ for $j = 1, 2, \ldots, 6$ and

$$\begin{aligned}L(a_1,a_2,\ldots,a_6,z) =&\frac{1}{2}\Bigg(\mathrm{Li}_2(z) + \mathrm{Li}_2(a_1^{-1}a_2^{-1}a_4^{-1}a_5^{-1}z) + \mathrm{Li}_2(a_1^{-1}a_3^{-1}a_4^{-1}a_6^{-1}) \\ &+ \mathrm{Li}_2(a_2^{-1}a_3^{-1}a_5^{-1}a_6^{-1}z) - \mathrm{Li}_2(-a_1^{-1}a_2^{-1}a_3^{-1}z) \\ &- \mathrm{Li}_2(-a_1^{-1}a_5^{-1}a_6^{-1}z) - \mathrm{Li}_2(-a_2^{-1}a_4^{-1}a_6^{-1}z) \\ &- \mathrm{Li}_2(-a_3^{-1}a_4^{-1}a_5^{-1}z) + \sum_{j=1}^{3}\log a_j \, \log a_{j+3}\Bigg),\end{aligned}$$

with $a_j = e^{i\theta_j}$ for $j = 1, \ldots, 6$, where θ_j are the dihedral angles of the tetrahedron. $\mathrm{Li}_2(z)$ is the dilogarithm function defined by a series expansion valid for $|z| \leq 1$

$$\mathrm{Li}_2(z) = \sum_{k=1}^{\infty} \frac{z^k}{k^2}\,. \tag{4.11}$$

We define $\tilde{L}(b_1,b_2,b_3,b_4,b_5,b_6,z) = L(-b_4^{-1},-b_5^{-1},-b_6^{-1},-b_1^{-1},-b_2^{-1},-b_3^{-1},z)$.

We now define the auxiliary parameter z_0 as

$$z_0 = \frac{-q_1 + \sqrt[2]{q_1^2 + 4q_0q_2}}{2q_2} \tag{4.12}$$

$$\begin{aligned}q_0 =&a_1a_4 + a_2a_5 + a_3a_6 + a_1a_2a_6 + a_1a_3a_5 + a_2a_3a_4 + a_4a_5a_6 + a_1a_2a_3a_4a_5a_6 \\ q_1 =&-(a_1 - a_1^{-1})(a_4 - a_4^{-1}) - (a_2 - a_2^{-1})(a_5 - a_5^{-1}) - (a_6 - a_6^{-1})(a_7 - a_7^{-1}) \\ q_2 =&a_1^{-1}a_4^{-1} + a_2^{-1}a_5^{-1}a_3^{-1}a_6^{-1} + a_1^{-1}a_2^{-1}a_6^{-1} + a_1^{-1}a_3^{-1}a_5^{-1} + a_2^{-1}a_3^{-1}a_4^{-1} + a_4^{-1}a_5^{-1}a_6^{-1} \\ &+ a_1^{-1}a_2^{-1}a_3^{-1}a_4^{-1}a_5^{-1}a_7^{-1}.\end{aligned}$$

Finally, we obtain $\tilde{z}_0$ and $\tilde{q}_2$ from z_0 and q_2 by substituting a_j with $-b_{j\pm3}^{-1}$ for $j = 1, \ldots, 6$. It is important to keep the same order of the edges as in figure 4.2.

Since computing the volume of each tetrahedron of the latice takes precious computing time, we prefer a faster method.

We did this by choosing a random unit vector $\vec{s}$. If this vector is inside the spherical tetrahedron spanned by the four spins $\{\vec{e}_1, \vec{e}_2, \vec{e}_3, \vec{e}_4\}$ of a single configuration of vertices, then this tetrahedron contributes to the topological charge with $dQ = \pm 1$. The sign of dQ is determined by the orientation of the spherical volume spanned by these 4 spins. This is done by taking the sign of the determinant of the matrix $[\vec{e}_1, \vec{e}_2, \vec{e}_3, \vec{e}_4]$. The topological charge is then the sum of the contributions dQ of each spherical tetrahedron spanned by all spins in the lattice:

$$Q = \sum_{\text{tetrahedron } i} dQ_i. \tag{4.13}$$

The topological charge cannot depend on the election of the random vector $\vec{s}$, and we can take it to be $\vec{s} = (1, 0, 0, 0)$. As a consistency test, we checked for a set of configurations that Q is indeed independent of the choice of $\vec{s}$, and coincides with the result obtained from Murakami's formula.

In order to probe whether if the vector $\vec{s}$ is indeed inside the spherical tetrahedron we must solve the following equation for $\vec{T}$

$$\vec{s} = [\vec{e}_1, \vec{e}_2, \vec{e}_3, \vec{e}_4]\vec{T}\,. \tag{4.14}$$

If all the components of $\vec{T}$ are positive, then $\vec{s}$ is inside the spherical tetrahedron. This method of computing the topological charge is by far the fastest one.

4.2 Results with $L = 8, 12, 16, 20$

We begin each simulatio with a "hot start" (a random configuration), perform $N_{\text{therm}} = 10^4$ sweeps of thermalisation, and then proceed to take measurements every $N_{\text{skip}} = 10$ sweeps. We used $N_{\text{meas}} = 5 \times 10^4$ measurements for statistics splitted into 5 jobs with 10^4 measurements each. The errors were obtained by

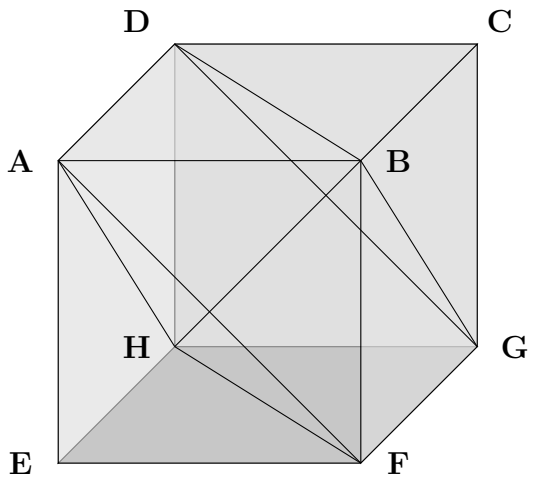

Figure 4.1: Decomposition of a single unit cube of the lattice into six tetrahedra.

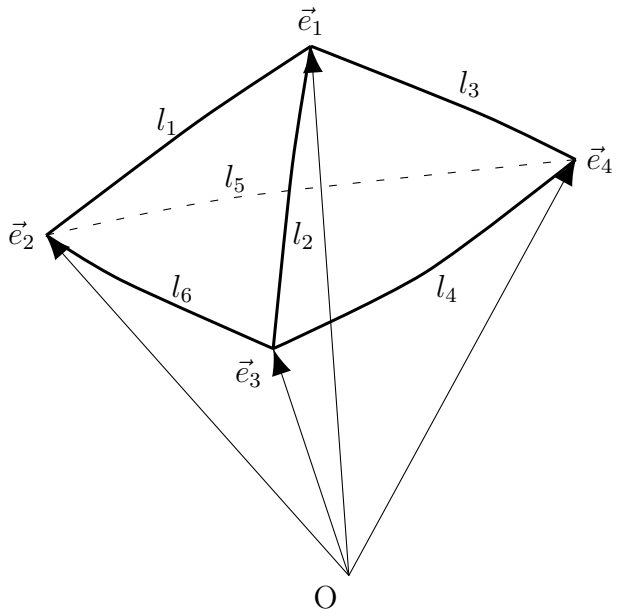

Figure 4.2: Spherical tetrahedron spanned by four spins $\{\vec{e}_1, \vec{e}_2, \vec{e}_3, \vec{e}_4\}$. The edges $l_1, \ldots, l_6$, are the shortest arcs in S^3.

the "jackknife" method using 5 bins, see Appendix A. The correlation length was obtained by equation (4.9) using a fit with GNUPLOT in the interval $[2, L-2]$ in order to exclude contaminations due to higher excitations. We used both the magnetic susceptibility and the specific heat to extract the crossover β_x by a 3-parameter fit to a Gaussian function

$$G(\beta) = A \exp\left[-\frac{1}{2}\left(\frac{\beta - \beta_x}{\sigma}\right)^2\right]. \tag{4.15}$$

We used both quantities to plot the crossover region in the phase diagram. We did this for every L we simulated, then we extrapolated β_x to $L \to \infty$ using a fit to a linear function

$$\beta_x(1/L) = \alpha\left(\frac{1}{L}\right) + \beta_x(0). \tag{4.16}$$

We also measure the autocorrelation function with respect ti the magnetization

$$ACF(t) = \langle [m(s) - \langle m\rangle]\,[m(t+s) - \langle m\rangle]\rangle \propto \exp\left(-\frac{t}{\tau_{\text{exp}}}\right) \tag{4.17}$$

to extract the exponential autocorrelation time τ_{exp}. For a discrete set of data we can approximate the normalized autocorrelation function as

$$ACF(t) = \frac{1}{(N_{\text{meas}} - t)\sigma^2} \sum_{k=1}^{N_{\text{meas}}-t} [m(k) - \langle m\rangle]\,[m(k+t) - \langle m\rangle]\ , \tag{4.18}$$

where $t = 0, \ldots, N_{\text{meas}} - 1$ and σ^2 is the variance of the data set.

The autocorrelation time is a measure of how long it takes to the system to move from one configuration to another which is significantly different, i.e. statistically independent. If we want truly independent configurations, we may want to take our measurements at intervals greater than one τ_{exp}. One can simply take measurements at intervals of $2\tau_{\text{exp}}$, see Ref. [14] for more details.

If we take N_{meas} measurements, the number of independent measurements after thermalization, is of the order of

$$n = \frac{N_{\text{meas}}}{2\tau_{\text{exp}}}\,. \tag{4.19}$$

4.2.1 Results at chemical potential $\mu_{B,\text{lat}} = 2$

We begin this section by analyzing the autocorrelation time in figure 4.3, to see whether we have a decent statistics or not. The largest value of τ_{exp} we have, is around 25 sweeps, according to equation (4.19) this leaves us a number of independent measurements of around $5 \times 10^4/(2.5 \times 2) = 10^4$ which are separated by 10 sweeps. Of course this number decreases as β_{lat} decreases. The lower τ_{exp} is around 10 sweeps, so we have a statistics of 2.5×10^4 independent measurements. We can say that we indeed have a decent statistics since at least we have between half and a fifth of the independent measurements left.

Figure 4.4 shows the time it took for the simulation to run a single job with 10^4 measurements separated by 10 Monte Carlo sweeps. We made a 2 parameter fit to a power law function $f(V) = \alpha V^\beta$ in order to predict the time at different volumes.

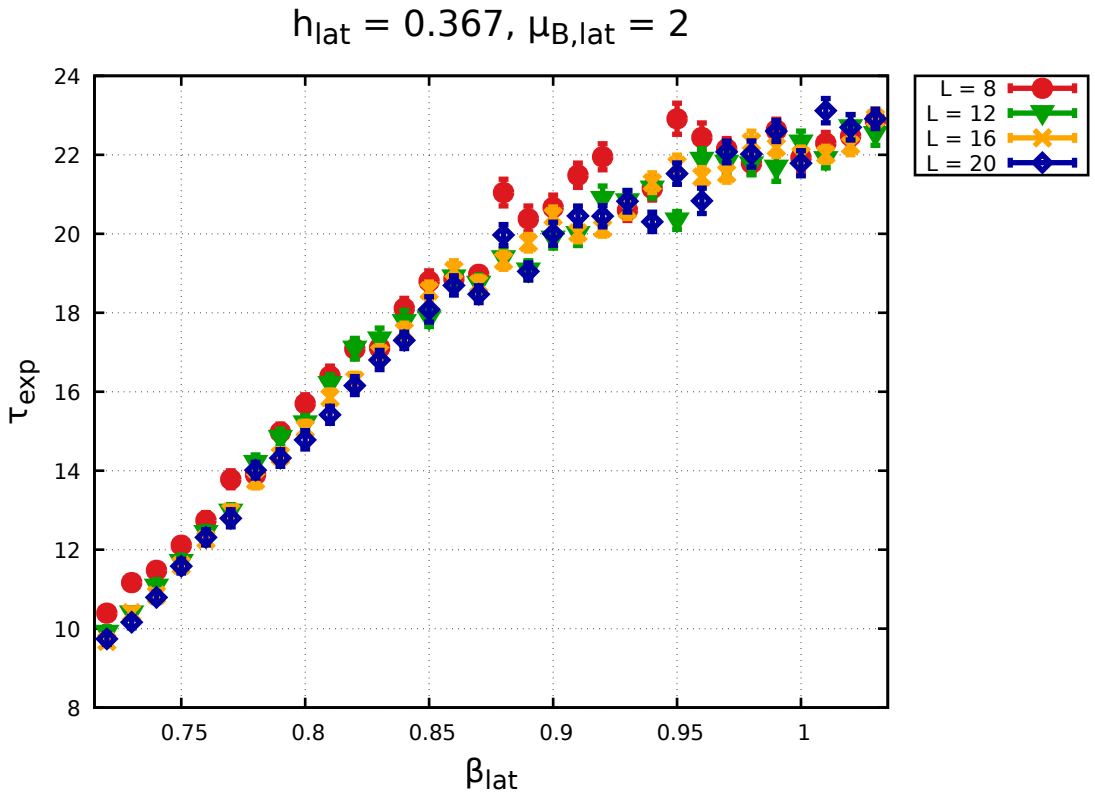

Figure 4.3: Exponential autocorrelation time in units of MC sweeps vs. β_{lat}.

In figure 4.5 we see the average size of the clusters of the Wolff algorithm. At high temperatures most of the clusters consist of a single spin. At low temperatures

the algorithm tends to create larger clusters. We see that the cluster size in small volumes is a bit larger than in extended volumes, this is due to the periodic boundaries. In small volumes a cluster is prone to close at the boundaries which makes it a bit larger.

Figure 4.6 is the acceptance rate of the flips of the Wolff algorithm with the modified flip probability.

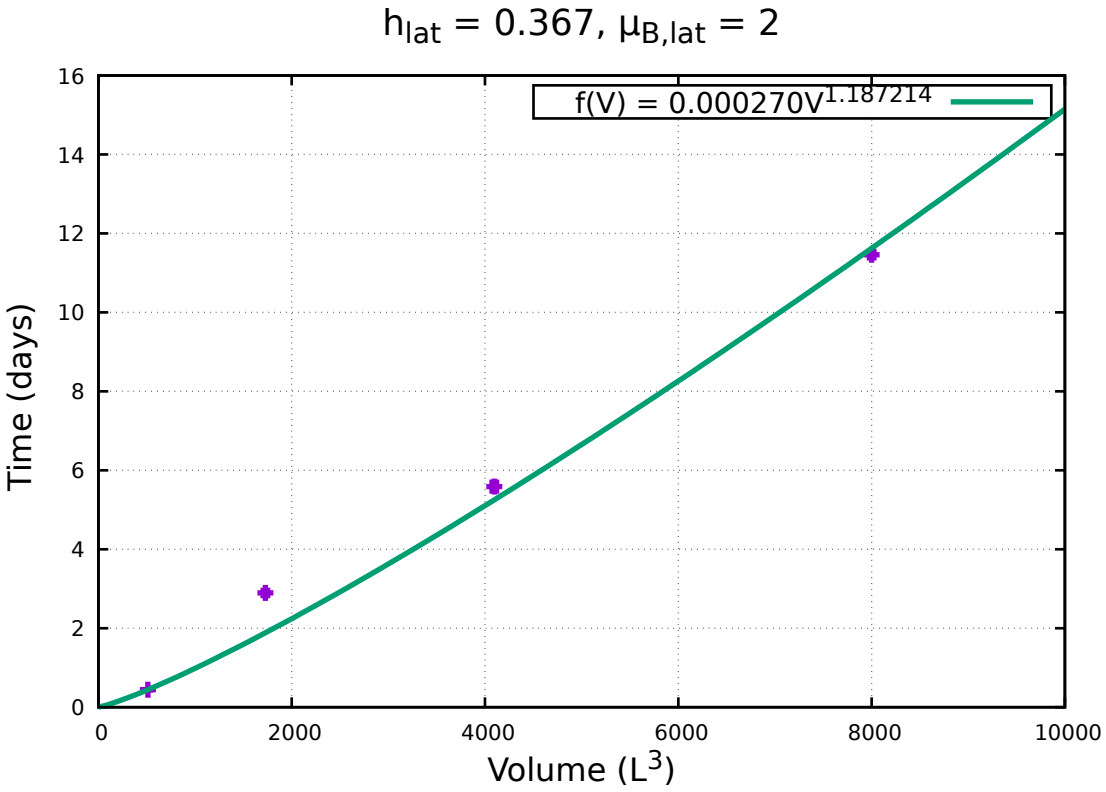

Figure 4.4: Average time in days of one single job with 10^4 measurements of statistics separated by 10 sweeps vs. the volume $V = L^3$ of the lattice. We include a fit to a power law. We used cores with a CPU clock speed of 2.40GHz.

Now we show plots for the observables defined earlier in this chapter. At this value of the chemical potential and at $L = 16$ we took 10^5 measurements instead of 5×10^4.

In figure 4.7 we see that the energy density of the system follows a smooth curve, which is stable in the volume. A way to tell if the system undergoes a first order phase transition is to look for discontinuities in some observables at β_c. In this case, the fact that we see a smooth curve agrees with the literature that indicate that the QCD phase diagram have whether a crossover or a first order

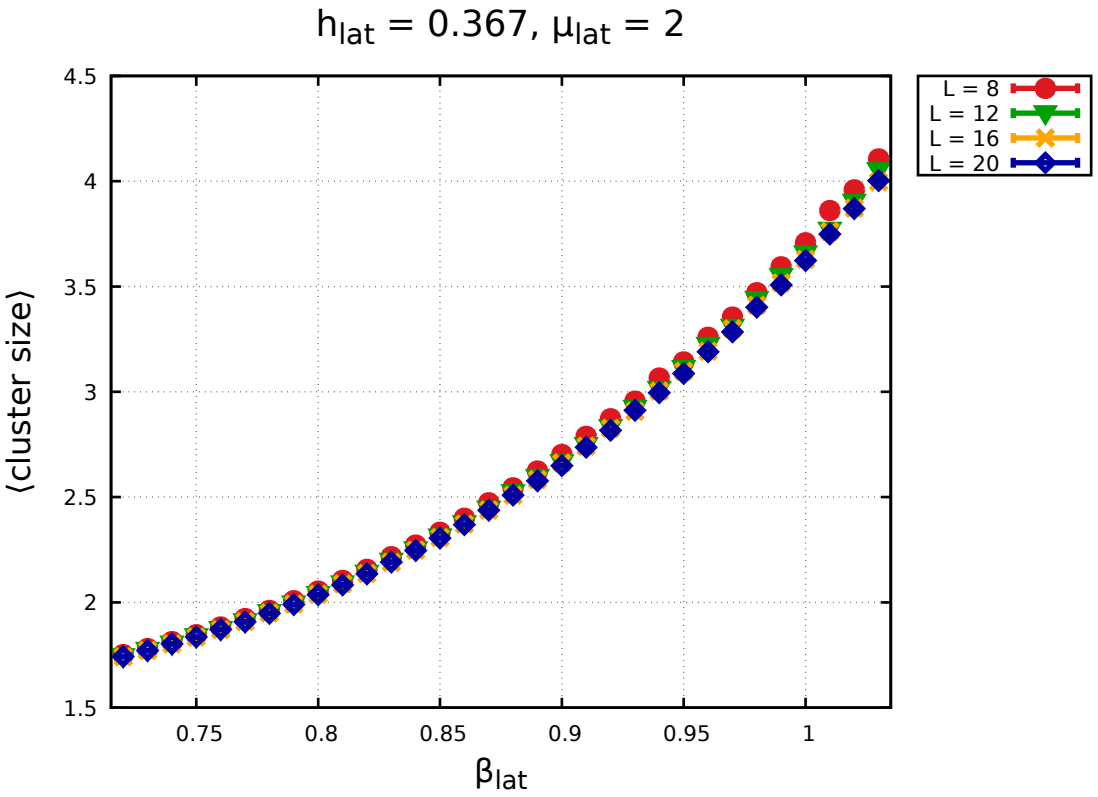

Figure 4.5: Average of the cluster size vs. β_{lat}.

phase transition, in our case we can say that we are in the crossover region.

Figure 4.8 shows the magnetization density. We see that it converges a bit slower than the energy density with increasing volume. Again, we observe a smooth behavior without any discontinuities.

Figure 4.9 shows the specific heat defined in equation (4.3). Although we observe that the peak increases at larger volumes, but this effect does not trend towards a divergence for $V \to \infty$, despite its peak gradually increasing. Therefore we can conclude that we are indeed in the crossover region. The fits using equation (4.15) are also shown to evaluate β_x in each volume. Figure 4.10 shows the β_x against the inverse of the lattice size L in order to extrapolate β_x to infinite volume, which is the value that we plot in the phase diagram.

Figures 4.11 and 4.12 show the magnetic susceptibility and the extrapolation of β_x to infinite volume. In the case of the specific heat we obtain $\beta_c = 0.950(15)$, but using the magnetic susceptibility we obtain $\beta_c = 0.793(2)$. This discrepancy in the values of β_c illustrates the fact that a crossover occurs in a region of the

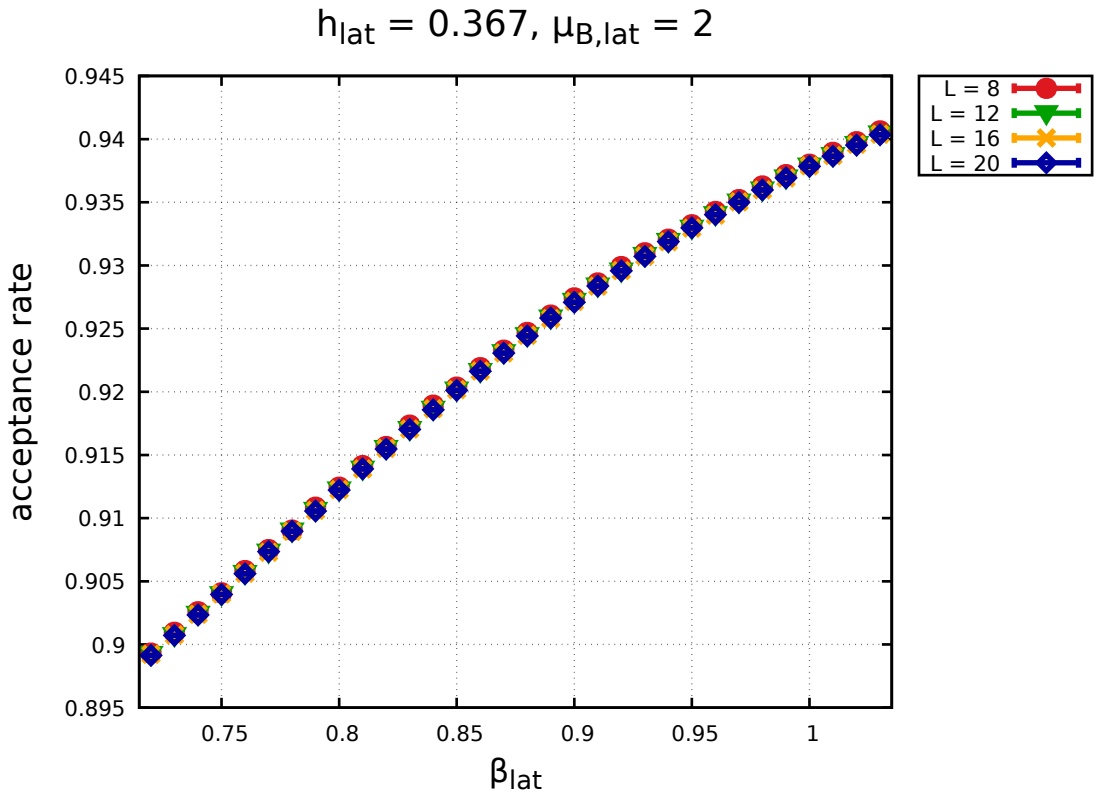

Figure 4.6: Acceptance rate of the flips vs. β_{lat}.

phase diagram rather than a single line.

Figure 4.13 depicts the topological charge density. It is also a smooth curve and for increasing volume. In figure 4.14 the topological susceptibility is shown: we see that at low β_{lat} this observable increases with increasing volume.

One of the most important quantities to measure is the correlation length ξ. This quantity set a physical scale of the system. We measured this by computing first the ξ for every single job, then we took the average and computed errors using the jackknife method with 5 bins.

4.2.2 Results at $L = 20$

We now show corresponding results at $\mu_{B,\text{lat}} \in \{0, 0.2, \ldots, 2\}$ with fixed volume $V = 20^3$.

In figure 4.16 we see that the autocorrelation time increases with increasing $\mu_{B,\text{lat}}$, This indicates that at higher values of the chemical potential, we can no longer rely on our statistics, which implies that we need to take more measurements

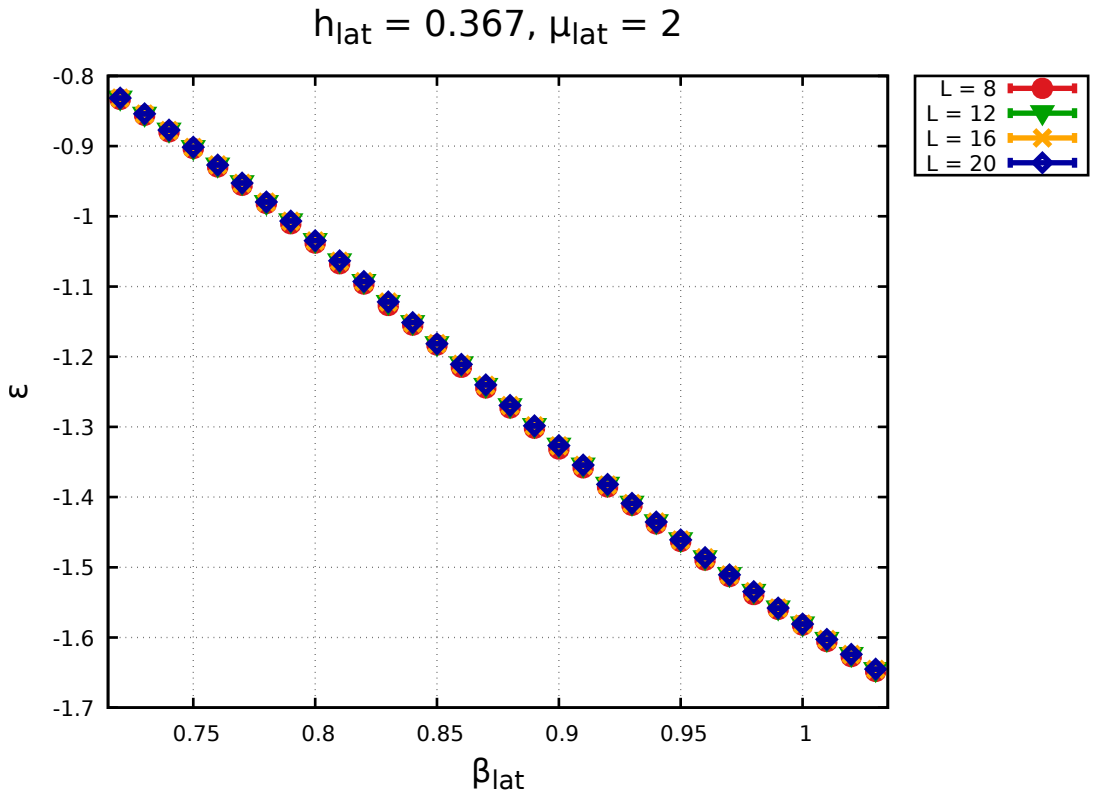

Figure 4.7: Energy density vs. β_{lat}.

at larger intervals.

In figure 4.19 we observe that the crossover $\beta_{x,\text{lat}}$ does not change when the chemical potential changes. So in our phase diagram we will obtained a crossover line which is almost constant in μ_B.

On the other hand, if we observe figure 4.20 we now see a change in $\beta_{x,\text{lat}}$, which will be reflected in the phase diagram of temperature vs. chemical potential as a decreasing line.

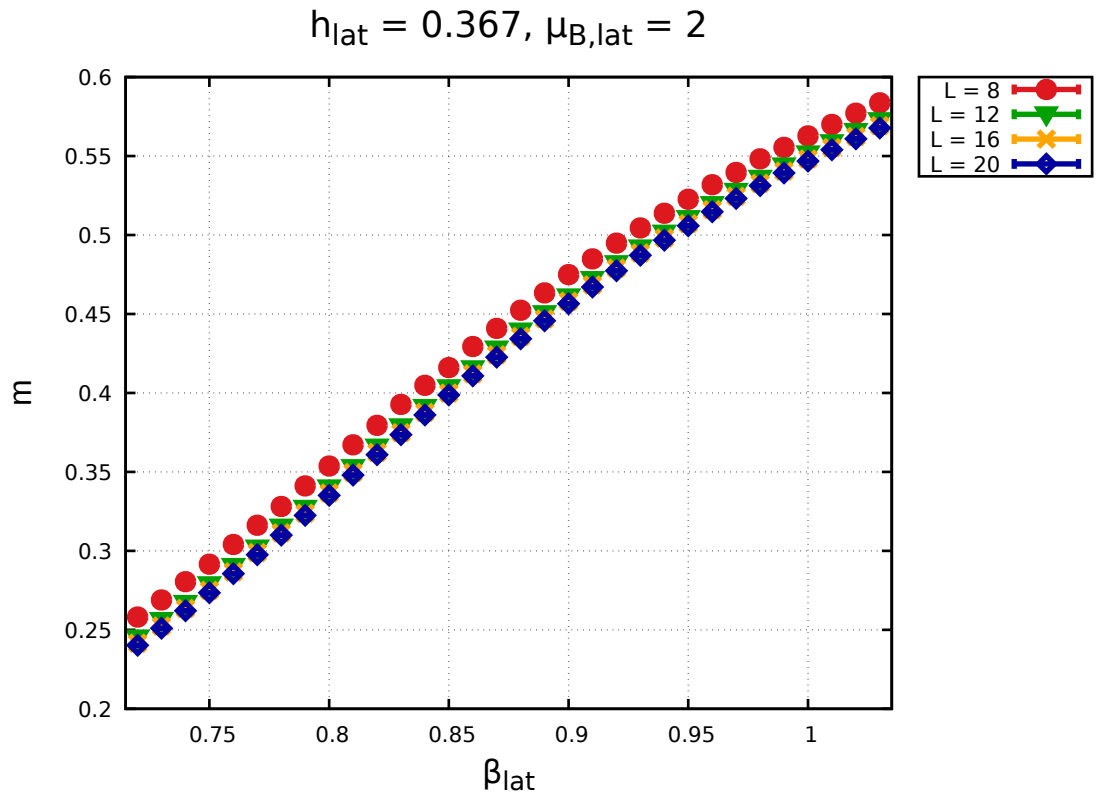

Figure 4.8: Magnetization density vs. β_{lat}.

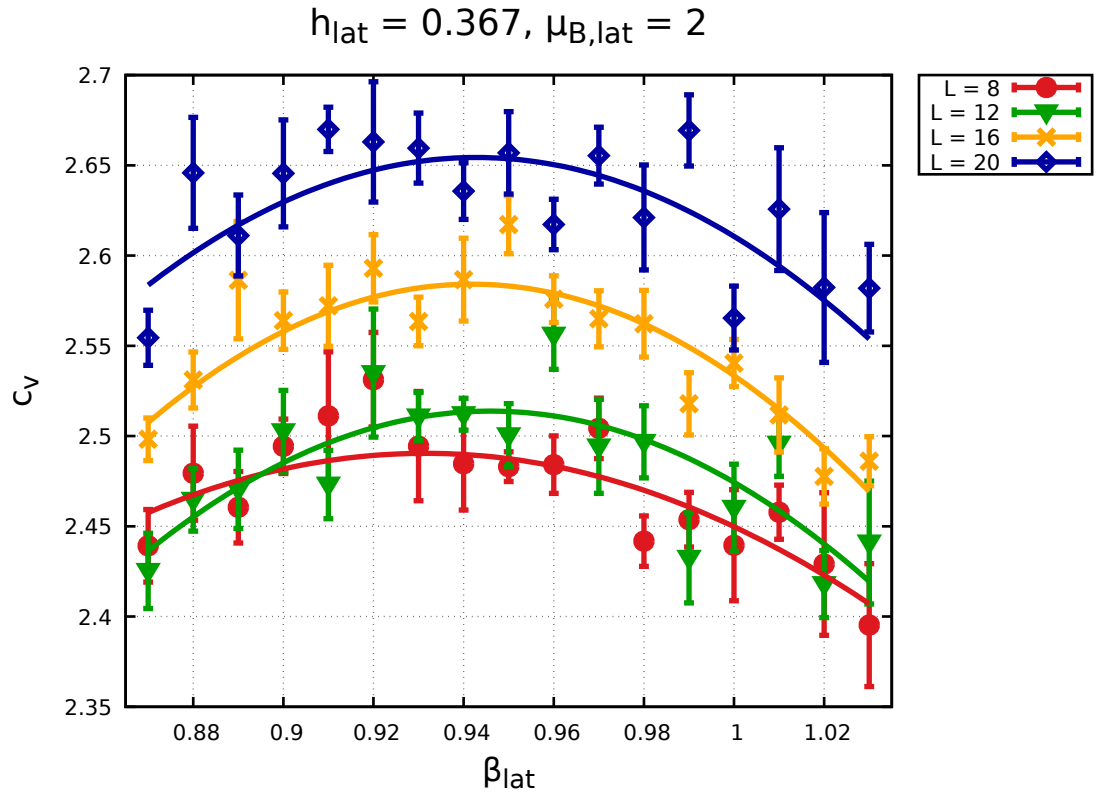

Figure 4.9: Specific heat vs. β_{lat}.

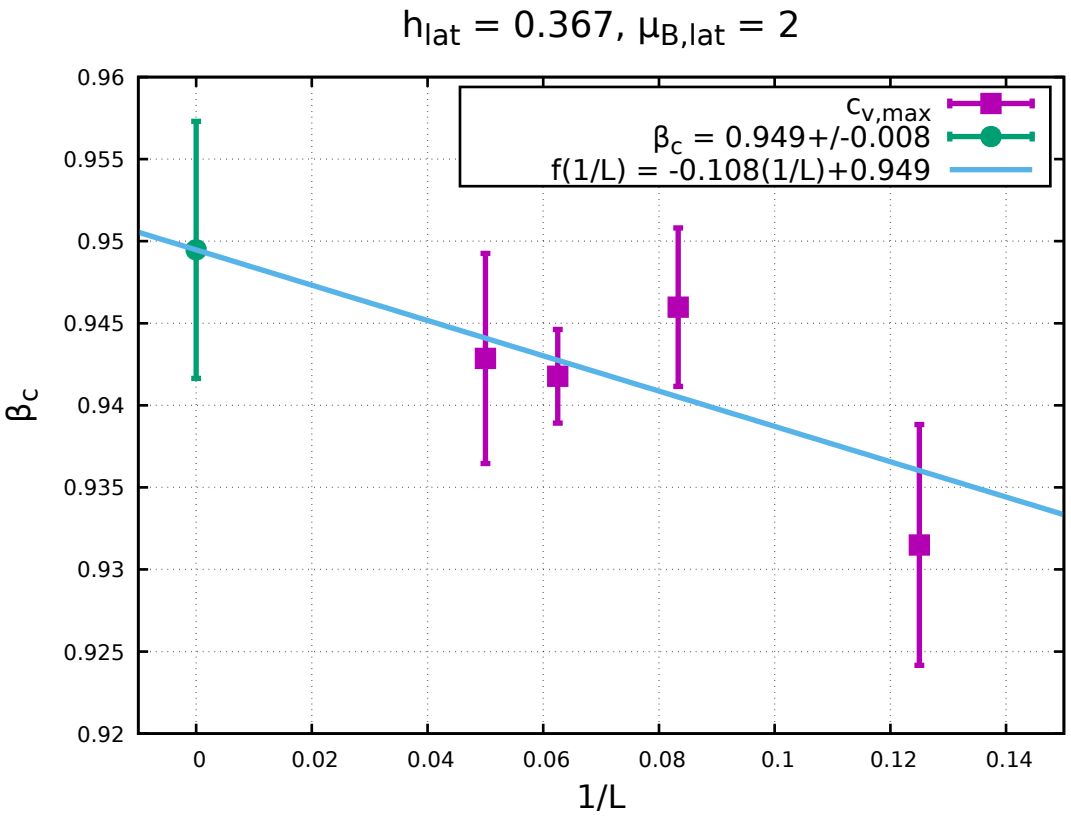

Figure 4.10: Fit of β_c extracted from the specific heat c_V at $L \to \infty$.

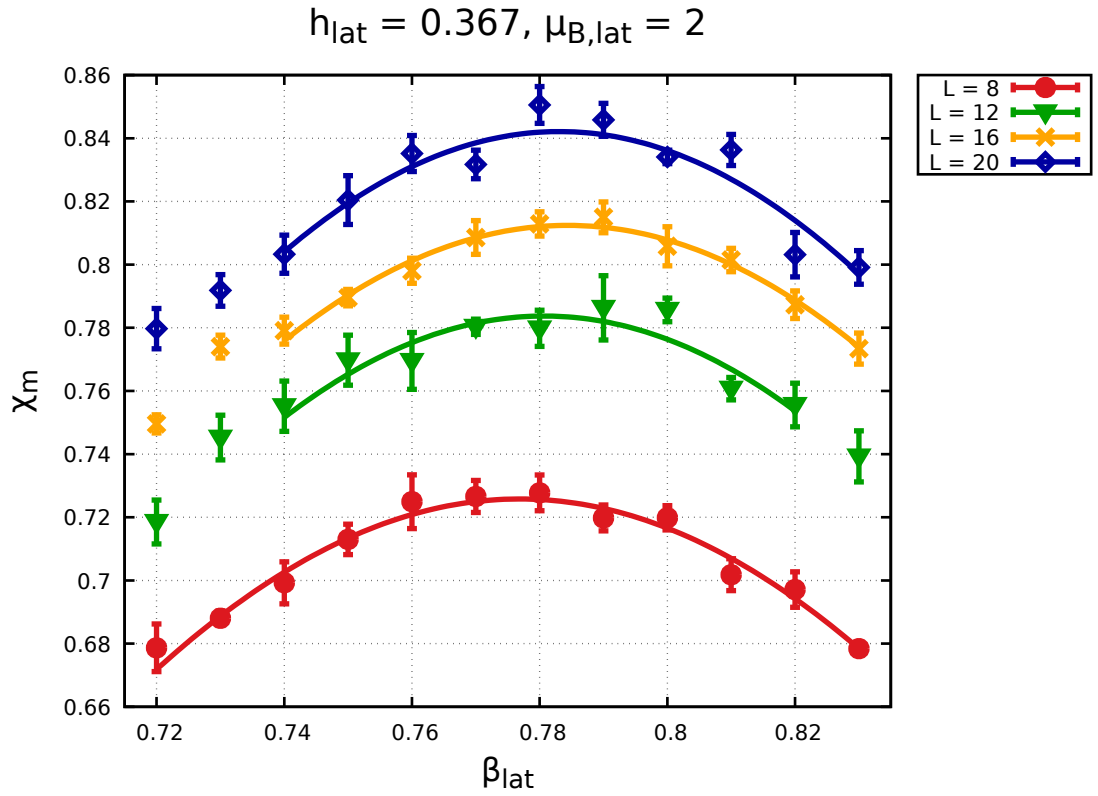

Figure 4.11: Magnetic susceptibility vs. β_{lat}.

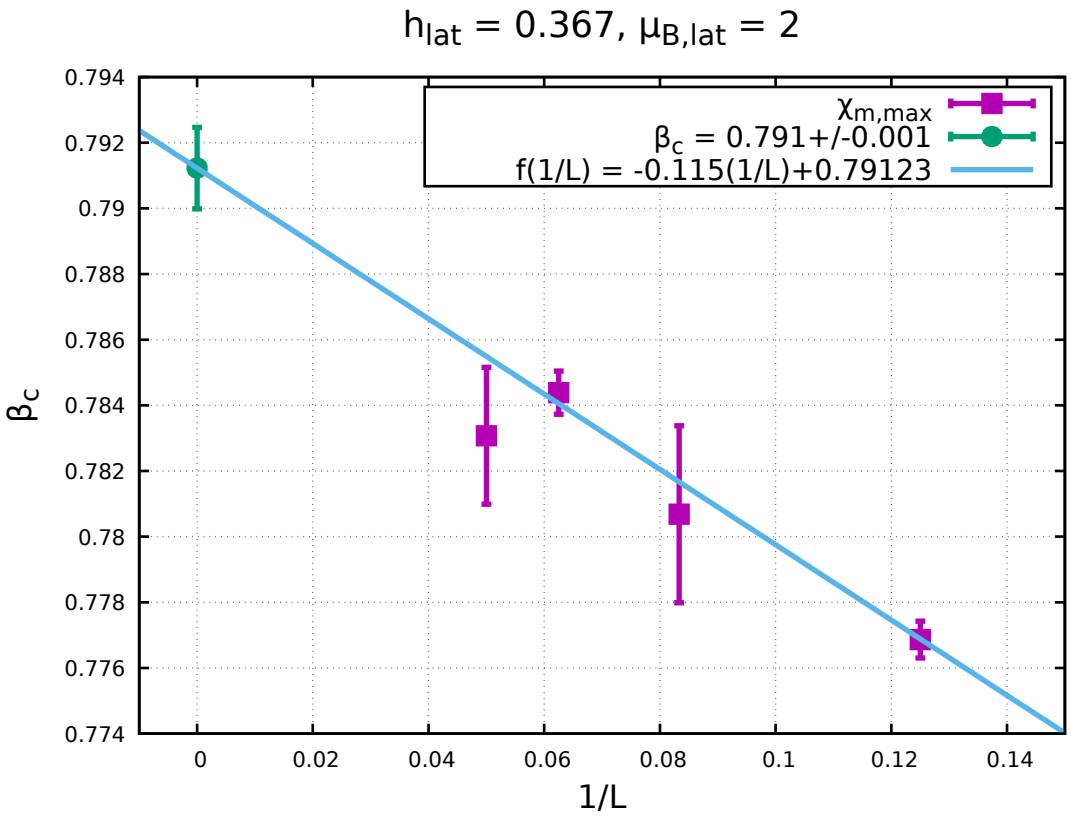

Figure 4.12: Fit of β_c extracted from the magnetic susceptibility χ_m at $L \to \infty$.

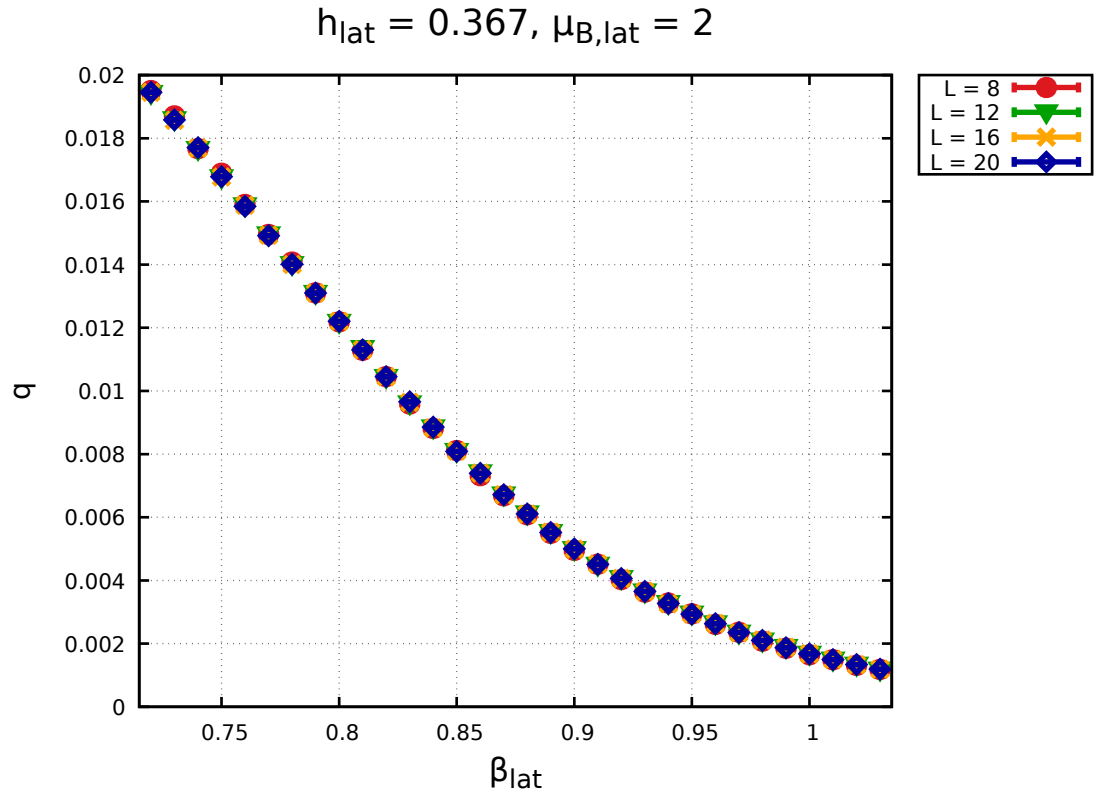

Figure 4.13: Topological charge density vs. β_{lat}.

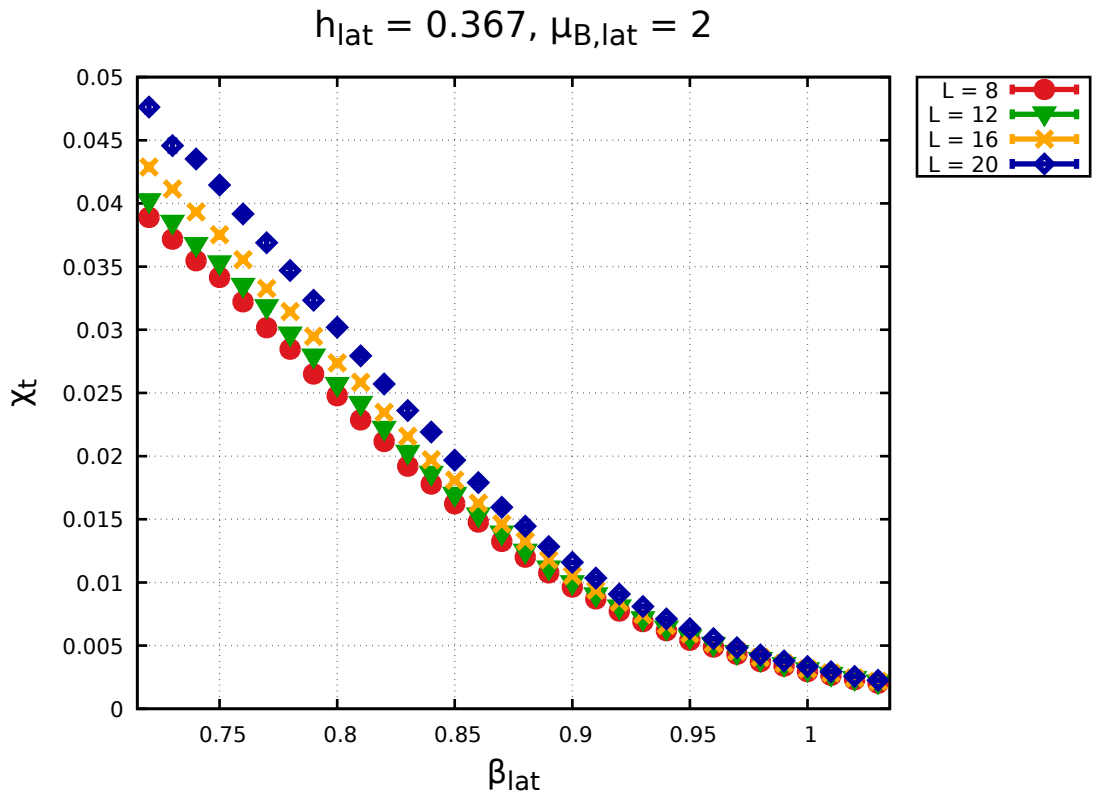

Figure 4.14: Topological susceptibility vs. β_{lat}.

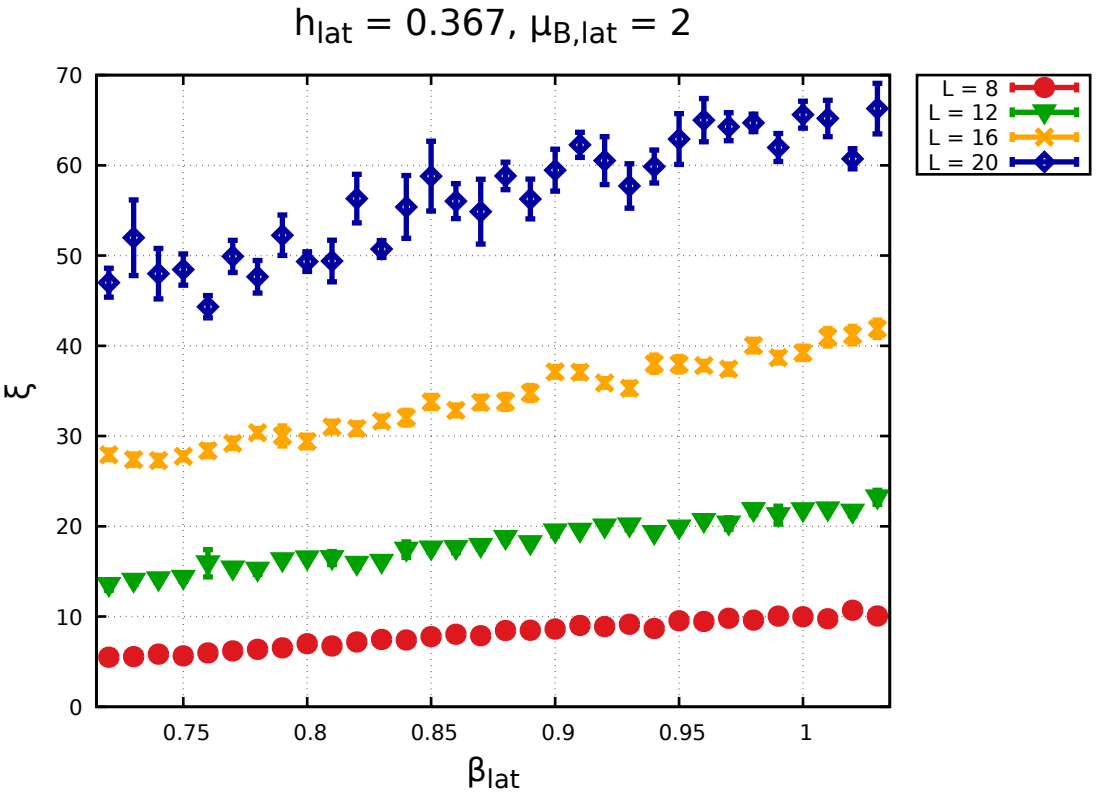

Figure 4.15: Correlation length vs. β_{lat}.

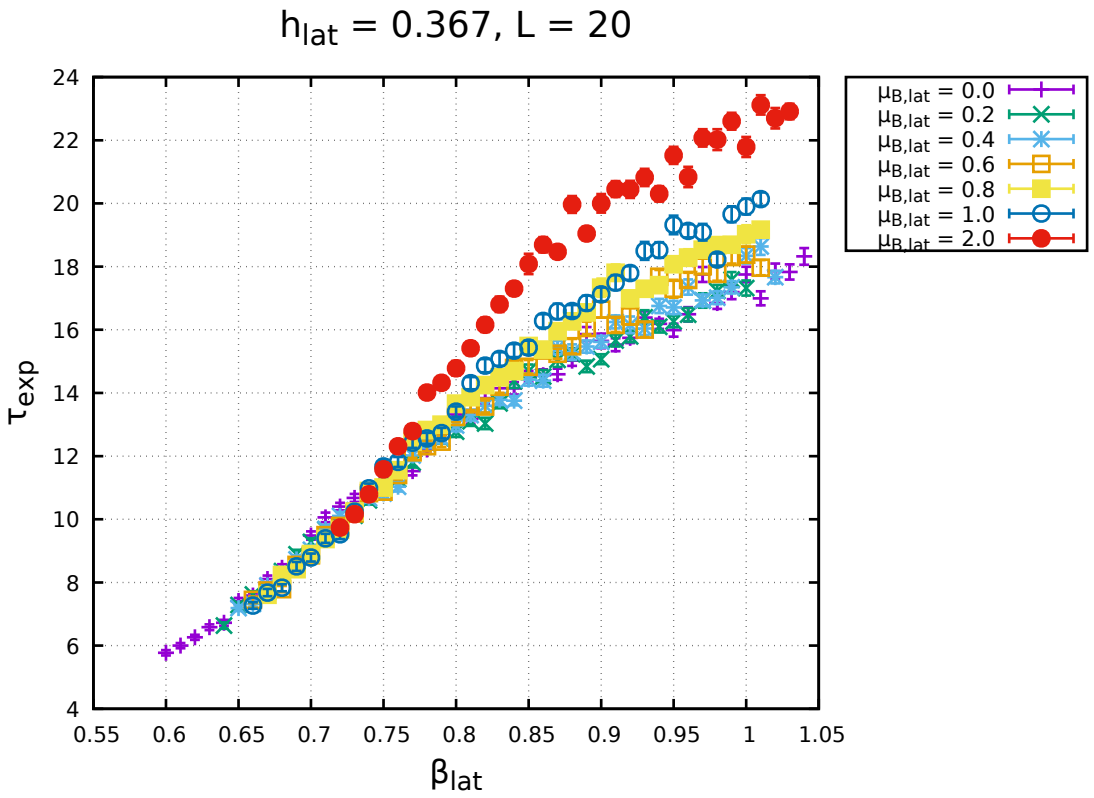

Figure 4.16: Exponential autocorrelation time in units of MC sweeps vs. β_{lat}.

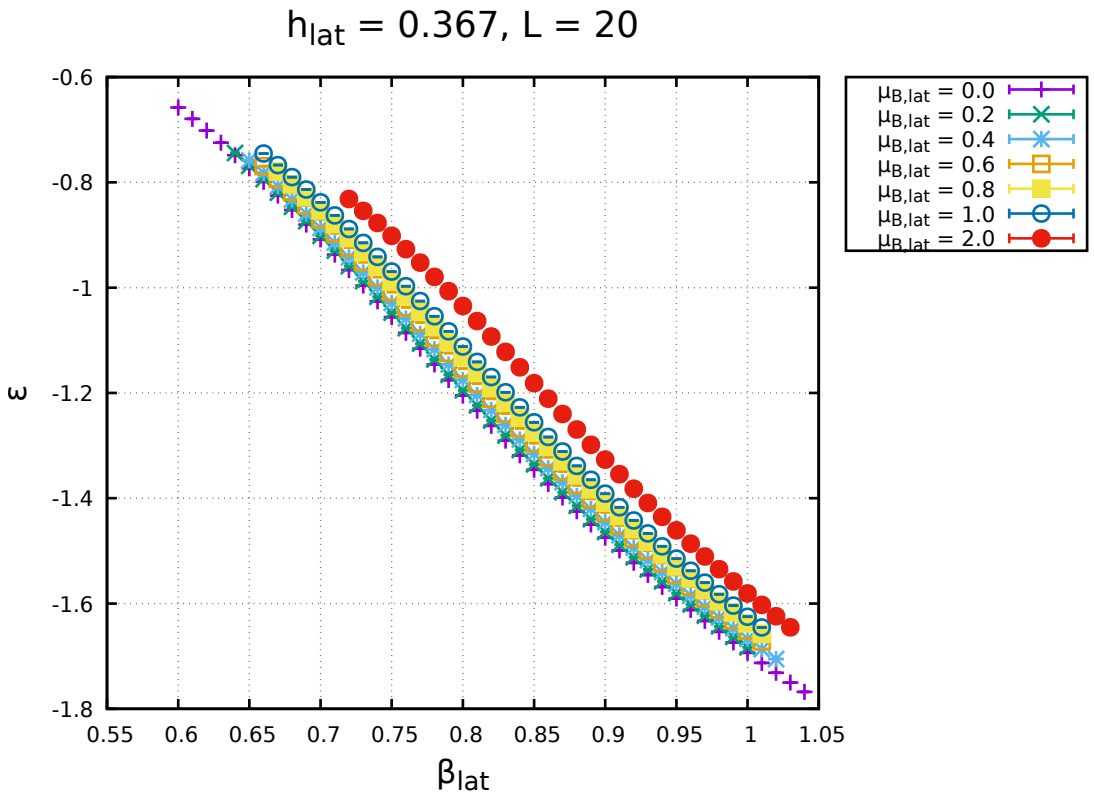

Figure 4.17: Energy density vs. β_{lat}.

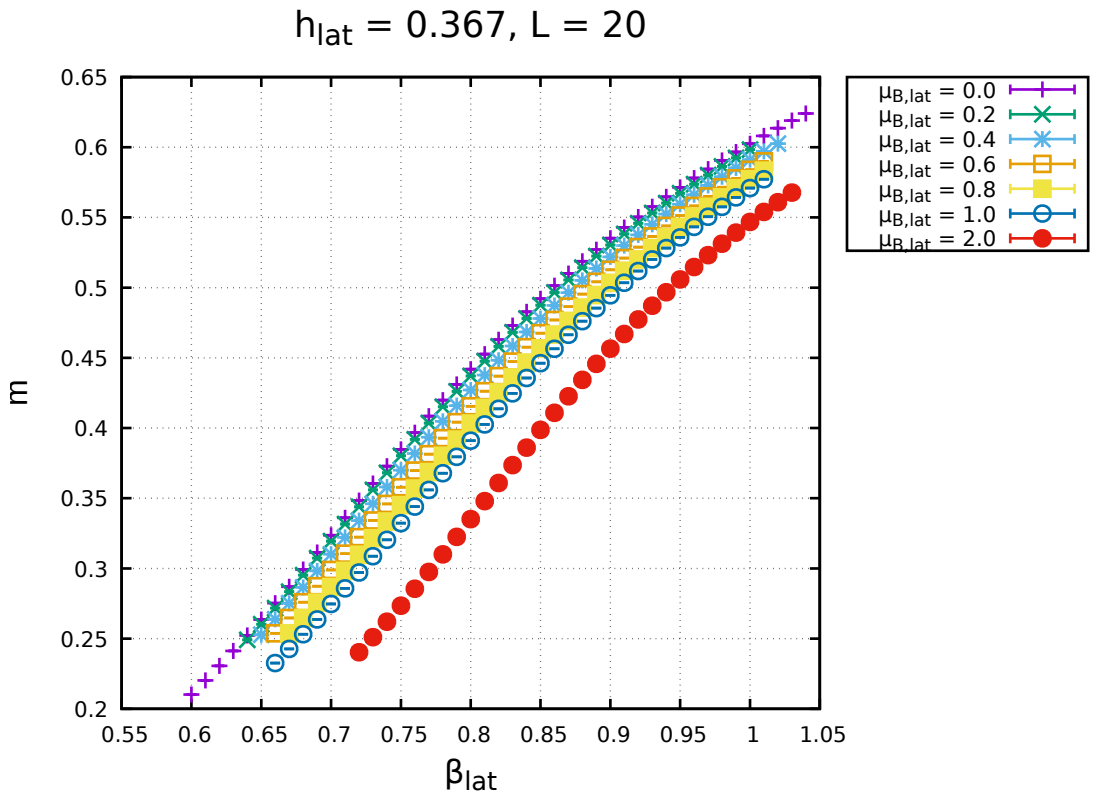

Figure 4.18: Magnetization density vs. β_{lat}.

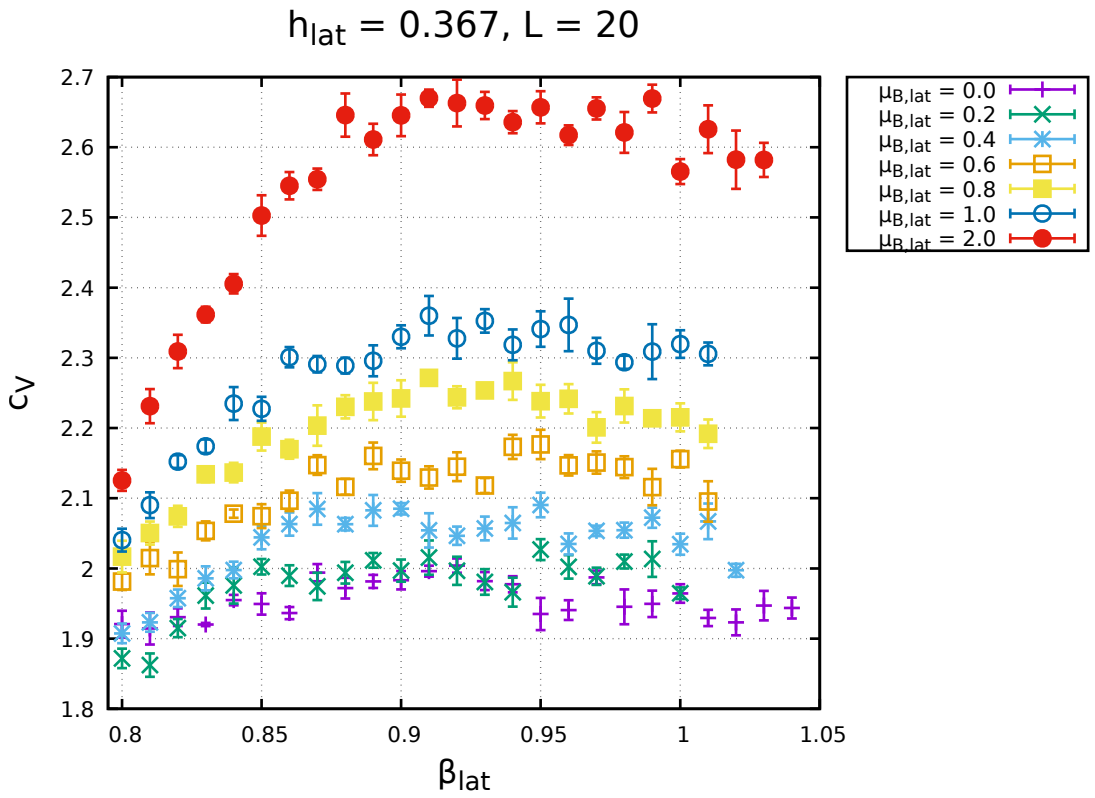

Figure 4.19: Specific heat vs. β_{lat}.

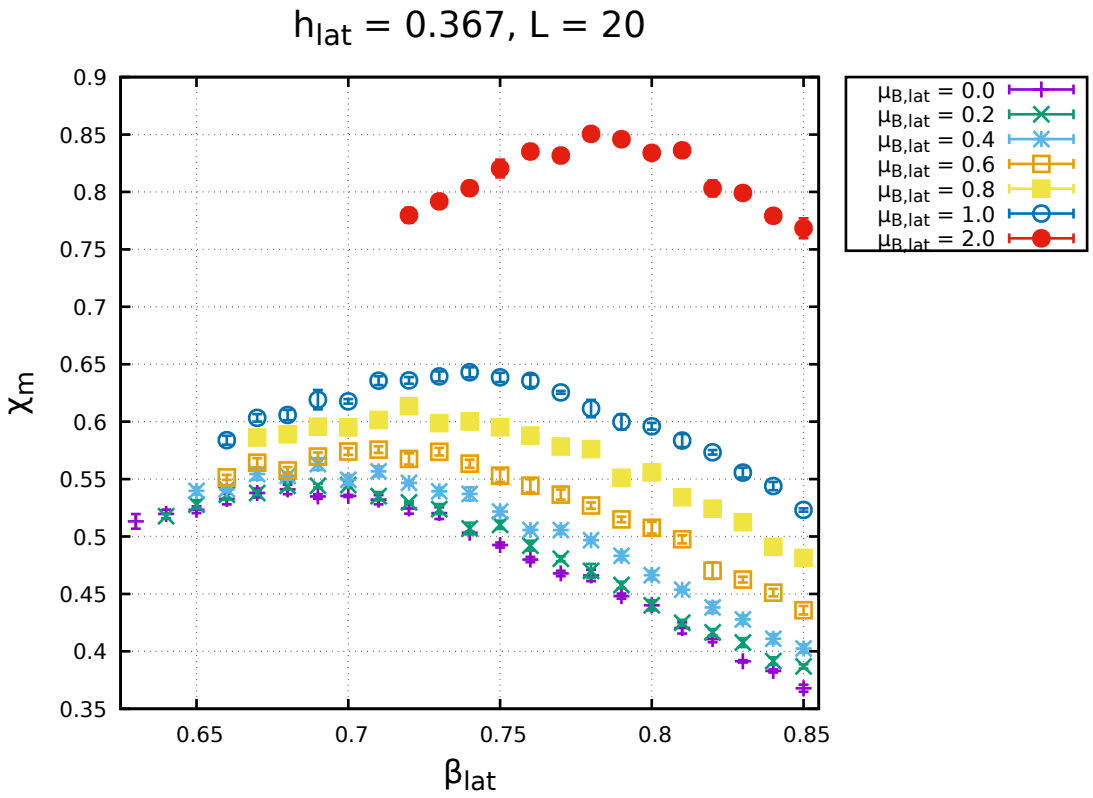

Figure 4.20: Magnetic susceptibility vs. β_{lat}.

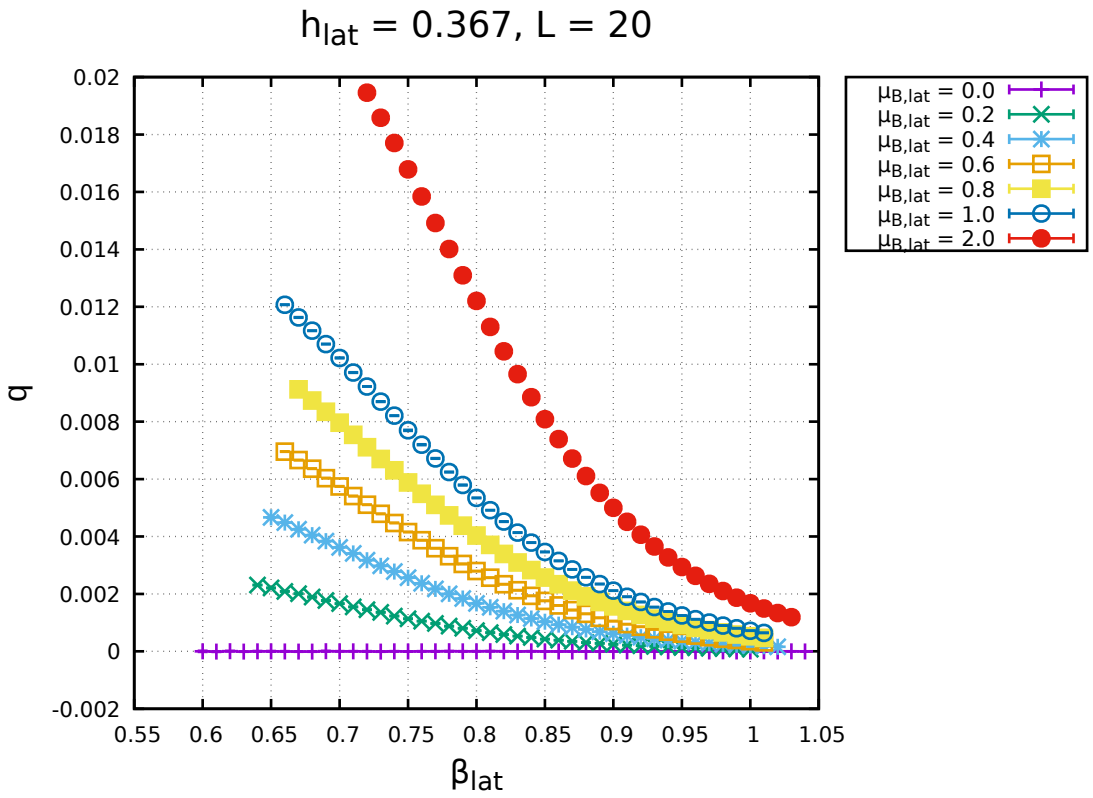

Figure 4.21: Topological charge density vs. β_{lat}.

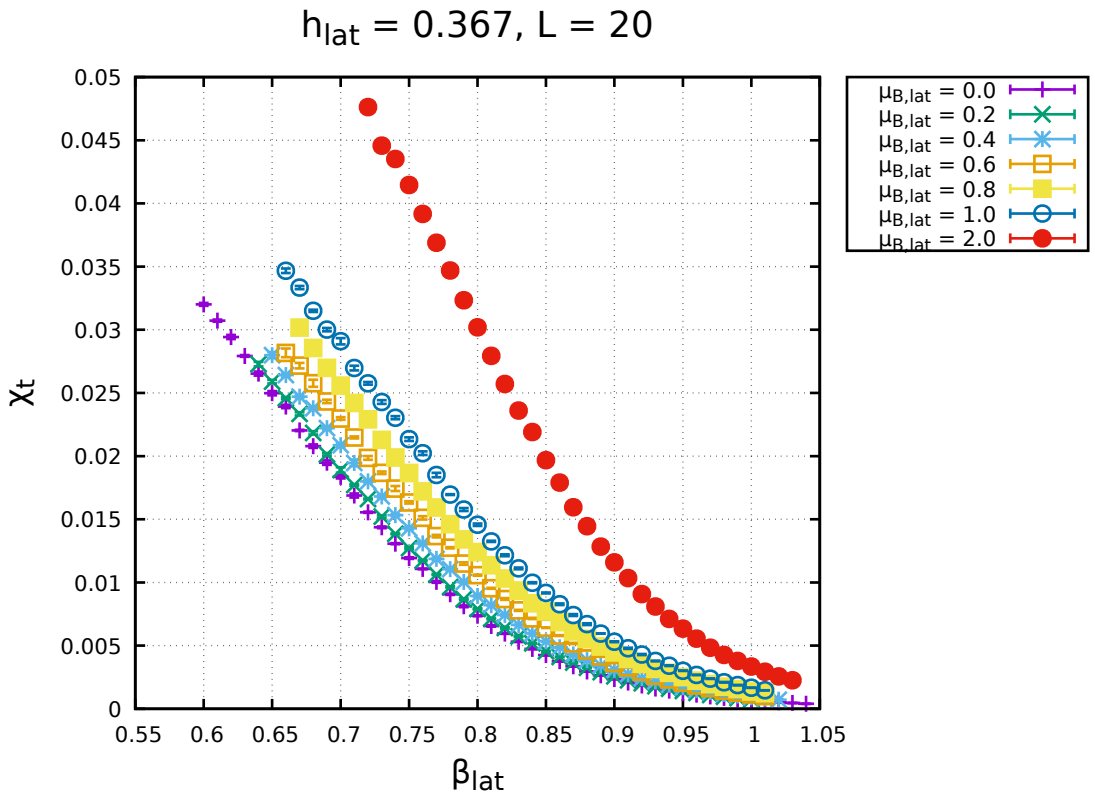

Figure 4.22: Topological susceptibility vs. β_{lat}.

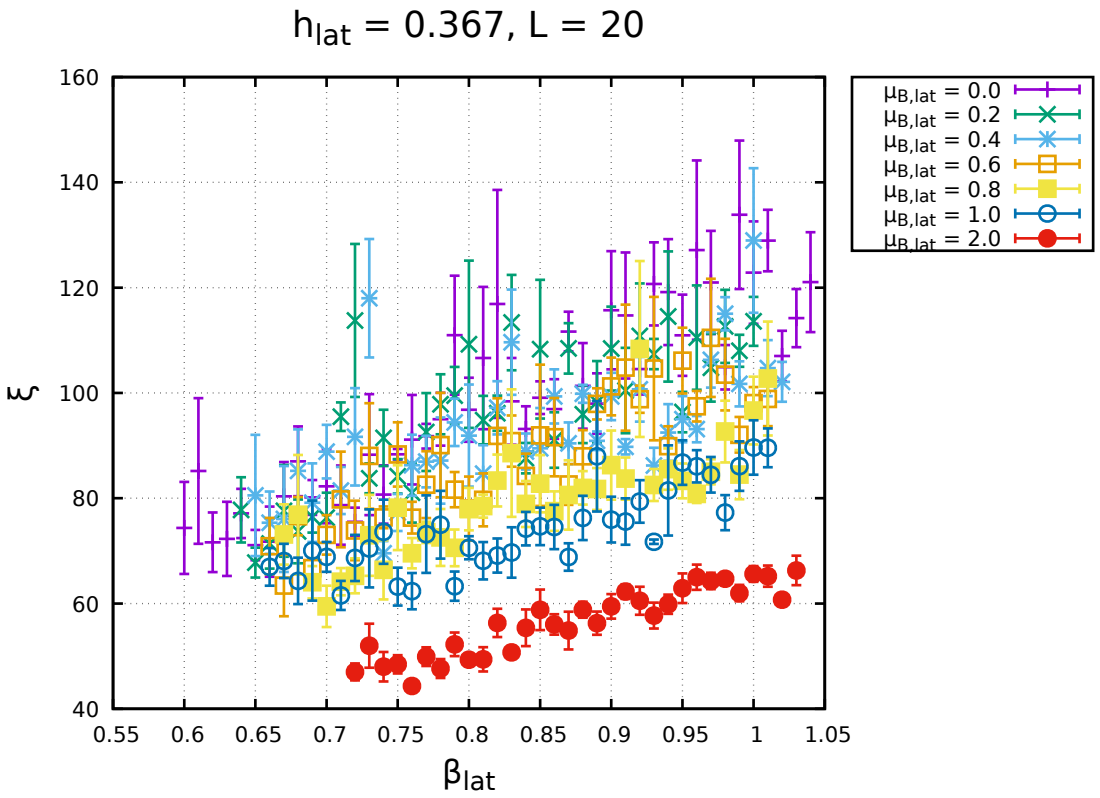

Figure 4.23: Correlation length vs. β_{lat}.

Chapter 5

Conclusions

In this work we explored the two flavor QCD phase diagram with massive quarks by studying the 3-d O(4) model. Since this model does not suffer from the sign problem, we could simulate the system at finite baryon density.

A variety of chemical potential, $\mu_{B,\mathrm{lat}}$ were simulated the system with different lattice volumes, $V = 8^3, 12^3, 16^3, 20^3$. We extracted the crossover temperatures $T_{x,\mathrm{lat}} = 1/\beta_{x,\mathrm{lat}}$ which we plot in the phase diagram, by extrapolating $\beta_{x,\mathrm{lat}}$ to infinite volume, using a Gaussian fit for the specific heat c_V and the magnetic susceptibility χ_m. Since the transition is a crossover, there is no single point which can be identified as the point where the transition actually takes place, instead there is a region which is given by c_v and χ_m. Without a chemical potential $\mu_{B,\mathrm{lat}} = 0$, the crossover occurs at $\beta_{x,\mathrm{lat}} = 0.931(8)$ for the c_V, and $\beta_{x,\mathrm{lat}} = 0.680(1)$ for the χ_m. In order to convert the chemical potential and the temperatures into physical units we took the average of these two, $\beta_{x,\mathrm{lat}} = 0.806(5)$, and the ratio between this and the physical value $\beta_x \approx \frac{1}{155\,\mathrm{MeV}}$

$$\frac{\beta_{x,\mathrm{lat}}}{\beta_x} \approx 125\,\mathrm{MeV}\,. \tag{5.1}$$

Finally we multiplied the temperature and the chemical potentials with this constant to obtain the physical values.

Figure 5.1 depicts the QCD phase diagram with two massive quark flavors. The red line is the crossover temperatures $T_x = 1/\beta_x$ using c_V and the green line using χ_m.

Reference	T_{CEP}	μ_{CEP}
[35]	$0.85T_c$	$1.11T_c$
[39]	69.9 MeV	319.1 MeV
[40]	5.1 MeV	286.7 MeV
[41]	144-155 MeV	$> 2\,T_{\text{CEP}}$
[36]	112 MeV	204 MeV
[37]	119-162 MeV	84-86 MeV
[38]	38 MeV	245 MeV
[42]		> 133.3 MeV
[43]	> 130 MeV	> 133.3 MeV
[44]	18-45 MeV	315-349 MeV
This work		> 250 MeV

Table 5.1: Estimations of CEP by some authors including ours. Table taken from Ref. [44].

The main goal of this work was to check whether the hypothetical critical end point exists or not. A CEP was not observed in the range of energies we worked with. Nonetheless, our effective theory successfully predicts the decreasing behavior of the crossover line at least with the line using the magnetic susceptibility.

With our data, we can at least give a lower bound for the CEP, $\mu_B = 250\,\text{MeV}$. If we rely in our effective model, we can discard some of the estimations for the CEP in table 5.1, such as the ones in references [35], [36], [37] and [38].

Higher chemical potentials μ_B are difficult to simulate, due to increasing autocorrelation time, which implies an increase in the computing time due to the need of taking the measurements at higher intervals in order to have decent statistics.

The main limitation of our effective theory is that the dimensional reduction requires high energy, where the 2-flavor approximation is questionable. In order to fix this need to include at least the quark s, which implies derivatives in the effective Lagrangian of higher orders. Including such term has the effect that the 3-d O(4) model is no longer feasible to study the QCD phase diagram.

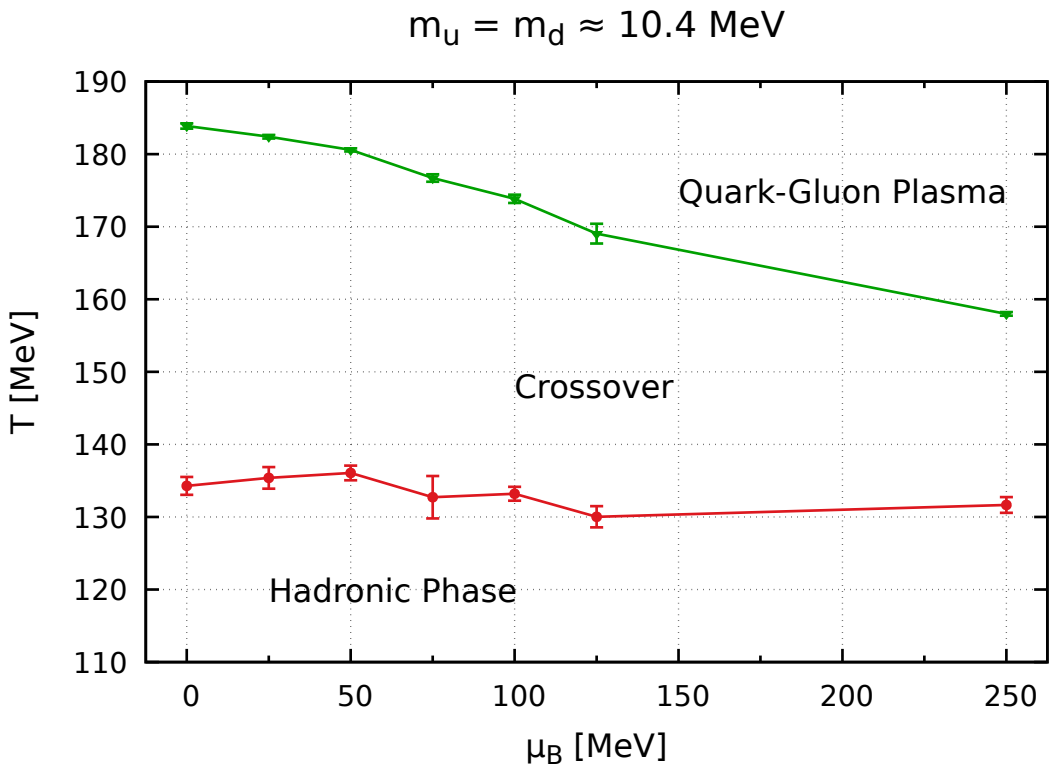

Figure 5.1: The two flavor QCD phase diagram with massive quarks, as conjectured from the 3-d O(4) model, which is expected to be in the same universality class.

Appendix A

Jackknife Error

Suppose a set of data of a certain quantity O with N elements is given. Then the jackknife error algorithm is specified by the following sequence of steps:

Jackknife method

1. Calculate the average $\bar{O}$ from the full data set.
2. Split the data set in M segments, or bins, with the same number of elements.
3. For each $m = 1, \ldots, M$ remove the m-th block and calculate the average $\bar{O}_{(m)}$ from the data of the $M - 1$ remaining blocks.
4. Estimate the error of O by

$$\delta O_{\text{jackknife}} = \sqrt{\frac{M-1}{M} \sum_{m=1}^{M} (\bar{O}_{(m)} - \bar{O})^2} \,.$$

Bibliography

[1] R. P. Feynman. Space-Time Approach to Non-Relativistic Quantum Mechanics. *Rev. Mod. Phys.*, 76:367–387, 1948.

[2] R.P. Feynman and A.R. Hibbs. *Quantum mechanics and path integrals*. International Series in Pure and Applied Physics. McGraw-Hill, 1965.

[3] J. S. Schwinger. A Theory of the Fundamental Interactions. *Annals Phys.*, 2:407–434, 1957.

[4] M. Gell-Mann and M. Lévy. The axial vector current in beta decay. *Nuovo Cim.*, 16:705–726, 1960.

[5] H. Nishimori and G. Ortiz. *Elements of Phase Transitions and Critical Phenomena*. Oxford Graduate Texts. OUP Oxford, 2011.

[6] N. D. Mermin and H. Wagner. Absence of Ferromagnetism or Antiferromagnetism in One- or Two-Dimensional Isotropic Heisenberg Models. *Phys. Rev. Lett.*, 17:1133–1136, 1966.

[7] S. R. Coleman. There are no Goldstone bosons in two-dimensions. *Commun. Math. Phys.*, 31:259–264, 1973.

[8] F. Englert and R. Brout. Broken Symmetry and the Mass of Gauge Vector Mesons. *Phys. Rev. Lett.*, 13:321–323, 1964.

[9] P. W. Higgs. Broken Symmetries and the Masses of Gauge Bosons. *Phys. Rev. Lett.*, 13:508–509, 1964.

[10] S. Sarkar, H. Satz, and B. Sinha. *The Physics of the Quark-Gluon Plasma: Introductory Lectures*. Lecture Notes in Physics. Springer Berlin Heidelberg, 2009.

[11] M. G. Alford, K. Rajagopal, and F. Wilczek. QCD at Finite Baryon Density: Nucleon Droplets and Color Superconductivity. *Phys. Lett.*, B422:247–256, 1998.

[12] D.J. Schwarz. The first second of the Universe. *Ann. Phys.*, 12:220–270, 2003.

[13] G. Baym, T. Hatsuda, Toru K., P. D. Powell, Y. Song, and T. Takatsuka. From Hadrons to Quarks in Neutron Stars: A Review. *Rept. Prog. Phys.*, 81:056902, 2018.

[14] M.E.J. Newman and G.T. Barkema. *Monte Carlo Methods in Statistical Physics*. Clarendon Press, 1999.

[15] N. Metropolis, A.W. Rosenbluth, M.N. Rosenbluth, A.H. Teller, and E. Teller. Equations of state calculations by fast computing machines. *J. Chem. Phys*, 21:1087–1091, 1953.

[16] R. H. Swendsen and J.-S. Wang. Nonuniversal Critical Dynamics in Monte Carlo Simulations. *Phys. Rev. Lett.*, 58:86–88, 1987.

[17] U. Wolff. Collective monte carlo updating for spin systems. *Phys. Rev. Lett.*, 62:361–364, 1989.

[18] J.-S. Wang. Clusters in the three-dimensional Ising model with a magnetic field. *Physica A Statistical Mechanics and its Applications*, 161:249–268, 1989.

[19] C. M. Fortuin and P. W. Kasteleyn. On the random-cluster model : I. Introduction and relation to other models. *Physica*, 57:536–564, 1972.

[20] K. Binder and D.W. Heermann. *Monte Carlo Simulation in Statistical Physics: An Introduction*. Graduate Texts in Physics. Springer Berlin Heidelberg, 2010.

[21] P. de Forcrand. Simulating QCD at finite density. *PoS*, LAT2009:010, 2009.

[22] J. Goldstone. Field Theories with Superconductor Solutions. *Nuovo Cim.*, 19:154–164, 1961.

[23] J. Goldstone, A. Salam, and S. Weinberg. Broken Symmetries. *Phys. Rev.*, 127:965–970, 1962.

[24] S. Weinberg. Phenomenological Lagrangians. *Physica A: Statistical Mechanics and its Applications*, 96:327 – 340, 1979.

[25] J. Gasser and H. Leutwyler. Chiral perturbation theory to one loop. *Annals of Physics*, 158:142 – 210, 1984.

[26] J. Gasser and H. Leutwyler. Chiral Perturbation Theory: Expansions in the Mass of the Strange Quark. *Nucl. Phys.*, B250:465–516, 1985.

[27] M. Gell-Mann, R. J. Oakes, and B. Renner. Behavior of Current Divergences under $SU_3 \times SU_3$. *Phys. Rev.*, 175:2195–2199, 1968.

[28] T. H. R. Skyrme. A nonlinear field theory. *Proc. Roy. Soc. Lond.*, A260:127–138, 1961.

[29] J. Engels, L. Fromme, and M. Seniuch. Correlation lengths and scaling functions in the three-dimensional O(4) model. *Nuc. Phys. B*, 675:533–554, 2003.

[30] M. Oevers. *The finite temperature phase diagram of 2-flavour QCD with improved Wilson fermions*. PhD thesis, Universität Biefeld, 1996.

[31] T. Bhattacharya, M. I. Buchoff, N. H. Christ, H.-T. Ding, R. Gupta, C. Jung, F. Karsch, Z. Lin, R. D. Mawhinney, G. McGlynn, S. Mukherjee, D. Murphy, P. Petreczky, D. Renfrew, C. Schroeder, R. A. Soltz, P. M. Vranas, and H. Yin. QCD Phase Transition with Chiral Quarks and Physical Quark Masses. *Phys. Rev. Lett.*, 113:082001, 2014.

[32] M. A. Nava Blanco, W. Bietenholz, and A. Fernández Téllez. Conjecture about the 2-flavour QCD phase diagram. *J. Phys. Conf. Ser.*, 912:012048, 2017.

[33] M. A. Nava Blanco. Estudio del diagrama fase de QCD con dos sabores usando el modelo 3d O(4). Master's thesis, Benemérita Universidad Autónoma de Puebla, 2019.

[34] J. Murakami. The volume formulas for a spherical tetrahedron. *Proc. Amer. Math. Soc.*, 140:3289–3295, 2012.

[35] Chao Shi, Yi-Lun Du, Shu-Sheng Xu, Xiao-Jun Liu, and Hong-Shi Zong. Continuum study of the QCD phase diagram through an OPE-modified gluon propagator. *Phys. Rev. D*, 93:036006, 2016.

[36] J. Knaute, R. Yaresko, and B. Kämpfer. Holographic QCD phase diagram with critical point from Einstein–Maxwell-dilaton dynamics. *Physics Letters B*, 778:419 – 425, 2018.

[37] F. Maintas X. Antoniou, N. Diakonos and C. Tsagkarakis. Locating the QCD critical endpoint through finite-size scaling. *Phys. Rev. D*, 97, 2018.

[38] Zhang J. Cui Z. and Zong H. Proper time regularization and the QCD chiral phase transition. *Sci. Rep.*, 7:45937, 2017.

[39] G. A. Contrera, A. G. Grunfeld, and D. Blaschke. Supporting the search for the CEP location with nonlocal PNJL models constrained by lattice QCD. 52:231, 2016.

[40] Takeru Yokota, Teiji Kunihiro, and Kenji Morita. Spectral functions in functional renormalization group approach – analysis of the collective soft modes at the QCD critical point –, 2016.

[41] S. Sharma. The QCD Equation of state and critical end-point estimates at O(μB6). *Nuc. Phys. A*, 967:728 – 731, 2017.

[42] P. Kovacs and G. Wolf. Phase diagram and isentropic curves from the vector meson extended Polyakov quark meson model, 2017.

[43] R. Rougemont, R. Critelli, J. Noronha-Hostler, J. Noronha, and C. Ratti. Dynamical versus equilibrium properties of the QCD phase transition: A holographic perspective. *Phys. Rev. D*, 96:014032, 2017.

[44] A. Ayala, S. Hernández-Ortiz, and L.A Hernández. QCD phase diagram from chiral symmetry restoration: analytic approach at high and low temperature using the linear sigma model with quarks. *Rev. Mex. Fis.*, 64:302–313, 2018.